nature chemical biology

Article

https://doi.org/10.1038/s41589-023-01464-6

Lis1 slows force-induced detachment of cytoplasmic dynein from microtubules

Received: 25 May 2022

Accepted: 29 September 2023

Published online: 02 November 2023

Check for updates

Emre Kusakci[1], Zaw Min Htet[2], Yuanchang Zhao[2,3], John P. Gillies[4], Samara L. Reck-Peterson[4,5,6] & Ahmet Yildiz[1,2,3]

Lis1 is a key cofactor for the assembly of active cytoplasmic dynein complexes that transport cargo along microtubules. Lis1 binds to the AAA+ ring and stalk of dynein and slows dynein motility, but the underlying mechanism has remained unclear. Using single-molecule imaging and optical trapping assays, we investigated how Lis1 binding affects the motility and force generation of yeast dynein in vitro. We showed that Lis1 slows motility by binding to the AAA+ ring of dynein, not by serving as a roadblock or tethering dynein to microtubules. Lis1 binding also does not affect force generation, but it induces prolonged stalls and reduces the asymmetry in the force-induced detachment of dynein from microtubules. The mutagenesis of the Lis1-binding sites on the dynein stalk partially recovers this asymmetry but does not restore dynein velocity. These results suggest that Lis1–stalk interaction slows the detachment of dynein from microtubules by interfering with the stalk sliding mechanism.

Cytoplasmic dynein-1 (dynein hereafter) is the primary motor responsible for motility and force generation towards the minus ends of microtubules[1]. Dynein transports membranous organelles, vesicles, messenger RNA and unfolded proteins towards the nucleus, drives retrograde transport in neurons and plays crucial roles in cell division[2]. Mutations that impair dynein function are linked to severe neurodegenerative and developmental disorders[3].

The core structural component of the dynein transport machinery is the dynein heavy chain (DHC), which is composed of the tail domain and the motor domain (Fig. 1a). The tail domain facilitates dimerization and recruits other associated chains. The motor domain forms a catalytic AAA+ ring that connects to the tail via the linker domain, and to the microtubule via a coiled-coil stalk[4,5] (Fig. 1a). ATP hydrolysis in the AAA+ ring is coupled to the swinging motion of the linker at the surface of the ring[1], which powers minus end-directed motility[6]. Nucleotide hydrolysis also controls the binding and release of the motor from the microtubule by altering the registry of the stalk coiled coils[7]. Dynein adopts an autoinhibited 'phi' conformation[8–10] and switches to an active conformation when it forms a complex with dynactin and an activating adaptor[11,12].

Lissencephaly-1 (Lis1) is a required cofactor for the recruitment of dynein to kinetochores, the nuclear envelope and the cell cortex, and for the initiation of dynein-mediated transport of a wide variety of cargos (reviewed in ref. 13). Heterozygous mutations in the *LIS1* gene lead to neuronal migration deficiency during embryonic brain development and cause the severe neurodevelopmental disease, lissencephaly[14]. Lis1 consists of a dimerization domain and a WD40 β-propeller domain. β-Propeller domains bind near the AAA3 site of the AAA+ ring and the base of the stalk (Fig. 1a)[15–17]. Recent studies proposed that Lis1 binding to the AAA+ ring facilitates the assembly of active dynein–dynactin–adaptor complexes by preventing dynein from adopting the phi conformation[18–21]. Structure-guided mutations showed that the Lis1–stalk interaction is important for the localization of dynein to the cortex of yeast cells[15,16], but it remains to be determined how this interaction affects the mechanism of dynein motility.

The comigration of Lis1 has been reported to substantially reduce the velocity of microtubule gliding or processive motility of yeast, pig and human dynein–dynactin in vitro[17–19,22–24]. Several models have been proposed to explain how Lis1 binding pauses or slows down dynein

[1]Graduate Group in Biophysics, University of California Berkeley, Berkeley, CA, USA. [2]Department of Molecular and Cell Biology, University of California Berkeley, Berkeley, CA, USA. [3]Physics Department, University of California Berkeley, Berkeley, CA, USA. [4]Department of Cellular and Molecular Medicine, University of California San Diego, La Jolla, CA, USA. [5]Department of Cell and Developmental Biology, University of California San Diego, La Jolla, CA, USA. [6]Howard Hughes Medical Institute, Chevy Chase, MD, USA. e-mail: yildiz@berkeley.edu

https://doi.org/10.1038/s41589-023-01464-6

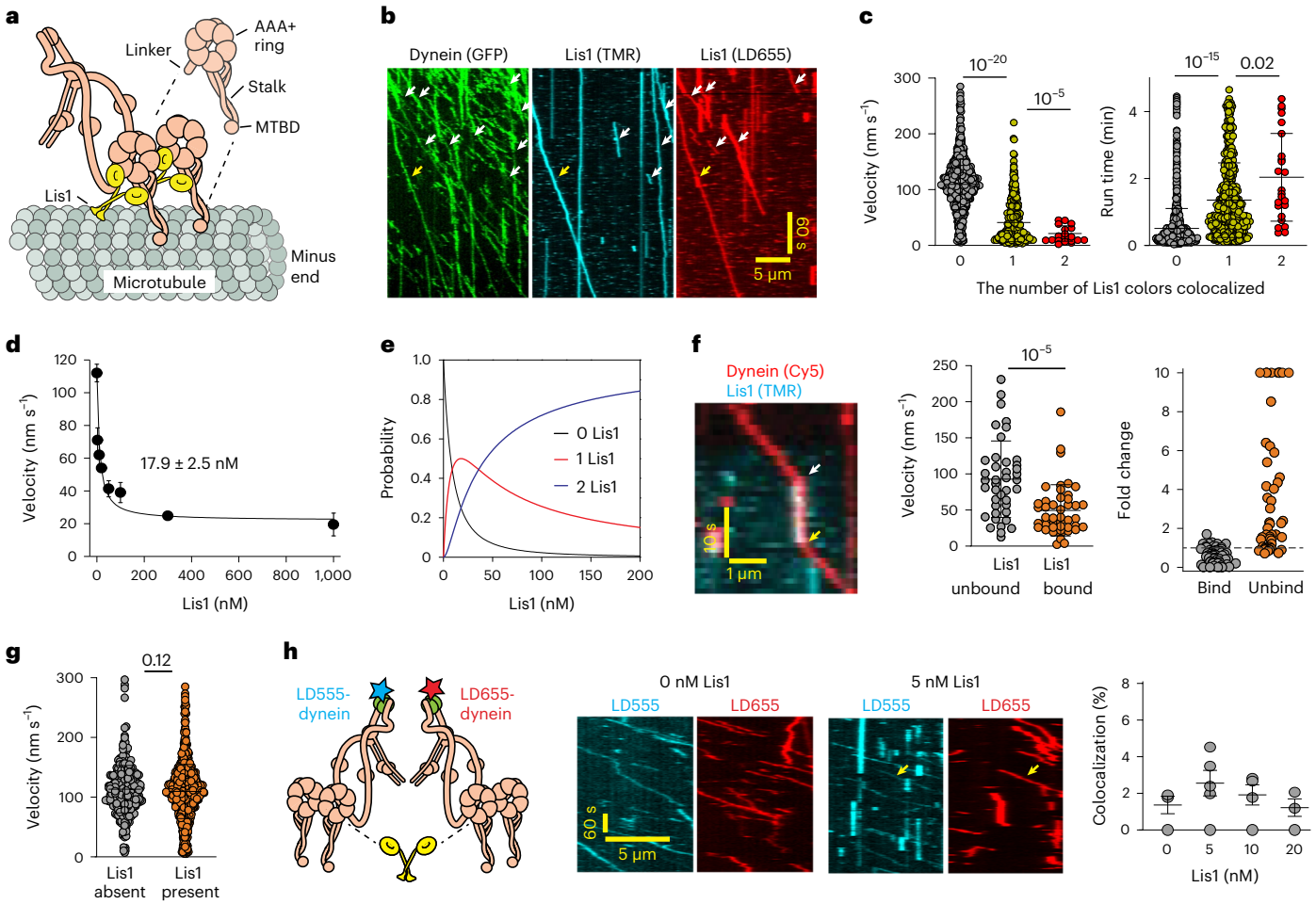

Fig. 1 | Lis1 binding reduces the velocity and increases the run time of dynein. **a**, Schematic of a Lis1-bound dynein on a microtubule. MTBD, microtubule-binding domain. **b**, A kymograph shows GFP-dynein colocalizes with one (white arrows) and two (yellow arrows) colors of Lis1 in the presence of 2 nM LD655- and 2 nM TMR-labeled Lis1. **c**, The velocity and run time of motors colocalized with 0, 1 and 2 colors of Lis1 (mean ± s.d., n = 1,530, 622 and 21 from left to right). **d**, Dynein velocity under different Lis1 concentrations in 50 mM KAc (mean ± s.e.m.; n = 861, 692, 288, 233, 352, 278, 312 and 131 from left to right; three biological replicates). The fit (solid curve) reveals K_d (±s.e.). **e**, The probability of 0, 1 and 2 Lis1 bound to dynein under different Lis1 concentrations. **f**, Transient binding (white arrow) and unbinding (yellow arrow) of Lis1 from dynein (left). The velocity of Lis1-unbound and Lis1-bound sections of dynein trajectories (mean ± s.d., n = 41 and 45 from left to right) (middle). The fold change in velocity upon Lis1 binding or unbinding (mean ± s.d., n = 64 and 47 from left to right) (right). **g**, The velocities of motors that do not colocalize with Lis1 with and without Lis1 in the chamber (n = 361 and 1,534, from left to right). **h**, Schematic shows whether a single Lis1 dimer can cross-bridge two dynein dimers labeled with different dyes (cyan and red stars) (left). Kymographs of 5 nM LD555-dynein (cyan) and 5 nM LD655-dynein (red) in 0 and 5 nM Lis1. Yellow arrows show colocalization between LD555 and LD655 (middle). The percentage of trajectories with colocalization between LD555 and LD655 (mean ± s.d.; n = 408, 378, 426 and 208 trajectories from left to right; three independent experiments) (right). See data analysis in Methods for curve fitting in **d** and **e**. In **c**, **f** and **g**, the center line and whiskers represent the mean and s.d., respectively. P values were calculated by a two-tailed t-test with Welch correction for velocity and by two-tailed Kolmogorov–Smirnov test for run time.

motility. Lis1 binding increases the microtubule-binding affinity of dynein[17,22,23,25], which may result in slower detachment of the motor domain before it can step along the microtubule. Cryo-electron microscopy of Lis1-bound dynein suggested that Lis1 clamps multiple AAA subunits together, trapping dynein in a conformation with high microtubule-binding affinity[15], possibly preventing rearrangements of the AAA subunits needed to switch to the low-affinity conformation. Lis1 binding to dynein has been proposed to inhibit or slow dynein by blocking the powerstroke of its linker domain[25]. A recent in vitro study proposed that Pac1 (the Lis1 homolog in budding yeast *Saccharomyces cerevisiae*, 'Lis1' hereafter) exerts a drag by tethering dynein to the microtubule in low ionic-strength buffers[20]. There are also reports that the Lis1 association increases[26] or does not affect[27] the velocity of human dynein–dynactin. Therefore, how Lis1 affects dynein velocity remains controversial.

In this study, we used single-molecule imaging and optical trapping to investigate how Lis1 binding affects the motility and force generation of yeast cytoplasmic dynein. Similar to mammalian dynein, Lis1 binding to yeast dynein prevents it from adopting the phi confirmation, and dynein mutants that cannot form the phi conformation partially rescue dynein function in yeast lacking Lis1 (ref. 20). Although yeast dynein also requires dynactin and a cortical attachment protein for its cellular function[28,29], it can walk processively in the absence of these cofactors[30] with similar stepping and force-generation properties to mammalian dynein–dynactin–adaptor complexes[31–35]. Therefore, yeast dynein serves as a simpler model to investigate how Lis1 binding affects the intrinsic motility and force-generation properties of dynein. Consistent with previous observations[17–19,36], we found that Lis1 binding slows dynein motility and induces longer run times on microtubules. Lis1 weakly interacts with microtubules, but this interaction does not slow dynein motility because Lis1 binding slows dynein even under conditions in which Lis1 does not interact with microtubules. Optical trapping assays revealed that Lis1 does not reduce the stall force, but results in slower microtubule detachment under hindering forces. Lis1

also decreases the asymmetry in the force-induced velocity of dynein. Mutations that disrupt the interactions of Lis1 with the dynein stalk partially restore the asymmetric detachment of dynein from microtubules in the presence of Lis1. These observations provide new insight into the mechanism of dynein regulation by Lis1.

Results

Lis1 binding stoichiometrically slows dynein motility

We expressed the full-length DHC (*DYN1*) with an amino-terminal GFP tag and a carboxy-terminal HaloTag from its endogenous locus in an *S. cerevisiae* strain lacking the genes encoding Lis1 (*PAC1*), the Lis-binding protein, NudEL (*NDL1*) and the p150 subunit of dynactin (*NIP100*; Supplementary Table 1). The DHC copurified with the endogenous dynein light intermediate chain (Dyn3), light chain (Dyn2) and intermediate chain (Pac11)[30]. We monitored the motility of this endogenously expressed complex (hereafter dynein) along microtubules in the presence and absence of Lis1 (Fig. 1a). To determine how Lis1 binding affects dynein motility, we separately labeled two different batches of Lis1 with TMR and LD655 dyes and monitored the colocalization of 2 nM TMR-Lis1 and 2 nM LD655-Lis1 with GFP-dynein. We observed either LD655-Lis1 or TMR-Lis1 translocating together with dynein on microtubules at similar colocalization percentages (14% each; Fig. 1b,c and Supplementary Video 1). A small fraction (1%) of GFP-dynein motors colocalized with LD655-Lis1 and TMR-Lis1 simultaneously, suggesting that a single dynein motor can recruit two Lis1 dimers (Fig. 1b), but this occurred rarely at low (2 nM) Lis1 concentrations[27]. Similar to mammalian dynein–dynactin–adaptor complexes[18,19], yeast dynein motors that colocalized with a single color of Lis1 moved slower (41 nm s^{-1}) and had a longer run time (81.4 s) on average than motors that did not colocalize with Lis1 (109 nm s^{-1} velocity and 30.5 s run time). Colocalization of both Lis1 colors further reduced the velocity (19 nm s^{-1}) and increased the run time (122.5 s) of dynein (Fig. 1c).

To estimate the affinity of Lis1 binding to processive dynein motors, we monitored dynein motility in the presence of 0–250 nM unlabeled Lis1 (Extended Data Fig. 1a–c). The average velocity of dynein under different Lis1 concentrations was fitted to the fraction of motors bound to 0, 1 and 2 Lis1 colors multiplied with their corresponding average velocities (Fig. 1d; see data analysis in Methods). The fit estimated that the dissociation constant of Lis1 (K_d) is 17.9 nM (Fig. 1d) and that most of the motors colocalize with two Lis1s at high Lis1 concentrations (Fig. 1e). We also observed that transient binding of Lis1 paused or slowed 83% of the motors, whereas unbinding of Lis1 increased the velocity of 77% of the motors, in agreement with previous observations on mammalian dynein[27] (Fig. 1f, Extended Data Fig. 1d and Supplementary Video 2). The velocity of dynein motors not colocalizing with Lis1 was similar to dynein velocity when there was no Lis1 in the chamber (Fig. 1g). Therefore, Lis1 slows dynein motility only when it is directly bound to the motor, and the presence of excess Lis1 in the chamber does not affect dynein velocity.

Previously, we proposed that human Lis1 facilitates the recruitment of two dyneins to the dynactin–adaptor complex by opening the autoinhibited phi conformation of dynein[18,19]. However, it is also possible that β-propeller domains of a Lis1 dimer cross-bridge the motor domains of two separate dynein dimers (Fig. 1h) and recruit them together to the dynactin–adaptor complex. To test this possibility, we differentially labeled two batches of dynein with LD555 and LD655 dyes and monitored their comigration on microtubules in the presence or absence of Lis1. Because the yeast strain that we purify endogenous dynein from lacks the *NIP100* gene, a functional dynactin complex should not be present in our assays, and colocalization of two dyneins could only be mediated by Lis1. In the absence of Lis1, we observed less than 1% colocalization between two different batches of 5 nM dynein labeled with LD555 and LD655. The presence of equimolar Lis1 to dynein led to only a marginal increase (2%) in colocalization between the differentially labeled dyneins (Fig. 1h), suggesting that Lis1 does not effectively cross-bridge two dyneins.

Lis1 slows dynein without interacting with microtubules

Unlike mammalian Lis1 (refs. 18,19), yeast Lis1 interacts with microtubules[20]. The degree to which Lis1 reduces dynein velocity was reported to correlate with the extent of Lis1–microtubule binding under different salt concentrations, indicating that yeast Lis1 may slow dynein by simultaneously binding dynein and the microtubule[20]. However, it is also possible that increasing the ionic strength of the buffer weakens the microtubule affinity of dynein. This could compete against the Lis1-mediated increase in the microtubule affinity of the motor, thereby reducing the effect of Lis1 in dynein velocity. We envisioned that the microtubule tethering model requires that: (1) either one Lis1 monomer interacts with dynein and the other monomer interacts with the microtubule; or (2) a single Lis1 monomer interacts simultaneously with both dynein and the microtubule (Fig. 2a). To test these models, we first characterized microtubule-binding dynamics of wild-type Lis1 dimer ($Lis1^{WT}$) and monomeric Lis1 lacking its amino-terminal dimerization domain ($Lis1^{monomer}$)[17]. As previously reported[20], $Lis1^{WT}$ decorated microtubules in 50 mM KAc (Fig. 2b,c). The fit to a binding isotherm revealed a K_d of 88 ± 8 nM (Extended Data Fig. 2a), which is higher than the K_d value we calculated from the Lis-mediated reduction of dynein velocity (Fig. 1d). Single $Lis1^{WT}$ stayed bound to the microtubule for 19.3 s on average and exhibited diffusive dynamics on the microtubule surface (Fig. 2d,e). However, there was little to no microtubule decoration of $Lis1^{WT}$ when the ionic strength of the buffer was increased to a physiologically relevant level (150 mM KAc; Fig. 2f,g)[20] or the carboxy-terminal tails of tubulin were cleaved by subtilisin[20] (Fig. 2h and Extended Data Fig. 2b). We concluded that Lis1 interacts with negatively charged tails of tubulin primarily through electrostatic interactions. However, this interaction is not strong enough to sustain microtubule binding in physiologically relevant salt concentrations, consistent with the lack of microtubule colocalization of Lis1 in yeast[37]. Compared to $Lis1^{WT}$, $Lis1^{monomer}$ exhibits little to no microtubule binding even under low salt conditions. $Lis1^{monomer}$ had a lower affinity for microtubules (Fig. 2b,c), only transiently interacted with microtubules and typically dissociated within 1–2 s (Fig. 2d,e).

We next measured the velocity of dynein in the presence of either $Lis1^{WT}$ or $Lis1^{monomer}$. The first model predicts that $Lis1^{monomer}$ would not affect the velocity of dynein. However, consistent with our previous observations[17], $Lis1^{monomer}$ slowed dynein motility in a dose-dependent manner (Fig. 2i), albeit not as strongly as $Lis1^{WT}$. Thus, if Lis1 cross-links dynein to microtubules, it must do so in the context of a monomer, with one face of Lis1 interacting with dynein and a different one interacting with microtubules. The second model predicts that mutants that disrupt Lis1 binding to dynein would not disrupt Lis1–microtubule binding, as the interfaces involved must be different. We tested this possibility by using dynein binding mutants of Lis1, in which a single ($Lis1^{R378A}$) or five ($Lis1^{5A}$) positively charged residues in the β-propeller domain were mutated to alanine (Extended Data Fig. 2c)[25]. Unlike $Lis1^{WT}$, $Lis1^{R378A}$ and $Lis1^{5A}$ were unable to decorate microtubules in 50 mM KAc (Fig. 2j and Extended Data Fig. 2d–e). $Lis1^{5A}$ also did not bind to microtubules in microtubule pelleting assays (Extended Data Fig. 2a), indicating that Lis1 interacts with microtubules through basic amino acids at the dynein-interacting surface of its β-propeller domain. Because a $Lis1^{monomer}$ would not be capable of cross-linking dynein to microtubules, but still slows dynein motility, our results are inconsistent with the microtubule tethering model.

While our results show that Lis1 binding to dynein is required to slow dynein motility (Fig. 1), it has been reported that the presence of Lis1 is sufficient to reduce the velocity of dynein motors that do not comigrate with Lis1 (ref. 20). This observation raises the possibility that Lis1 serves as a static obstacle against dynein motility on the microtubule surface, akin to microtubule-associated proteins[38,39].

https://doi.org/10.1038/s41589-023-01464-6

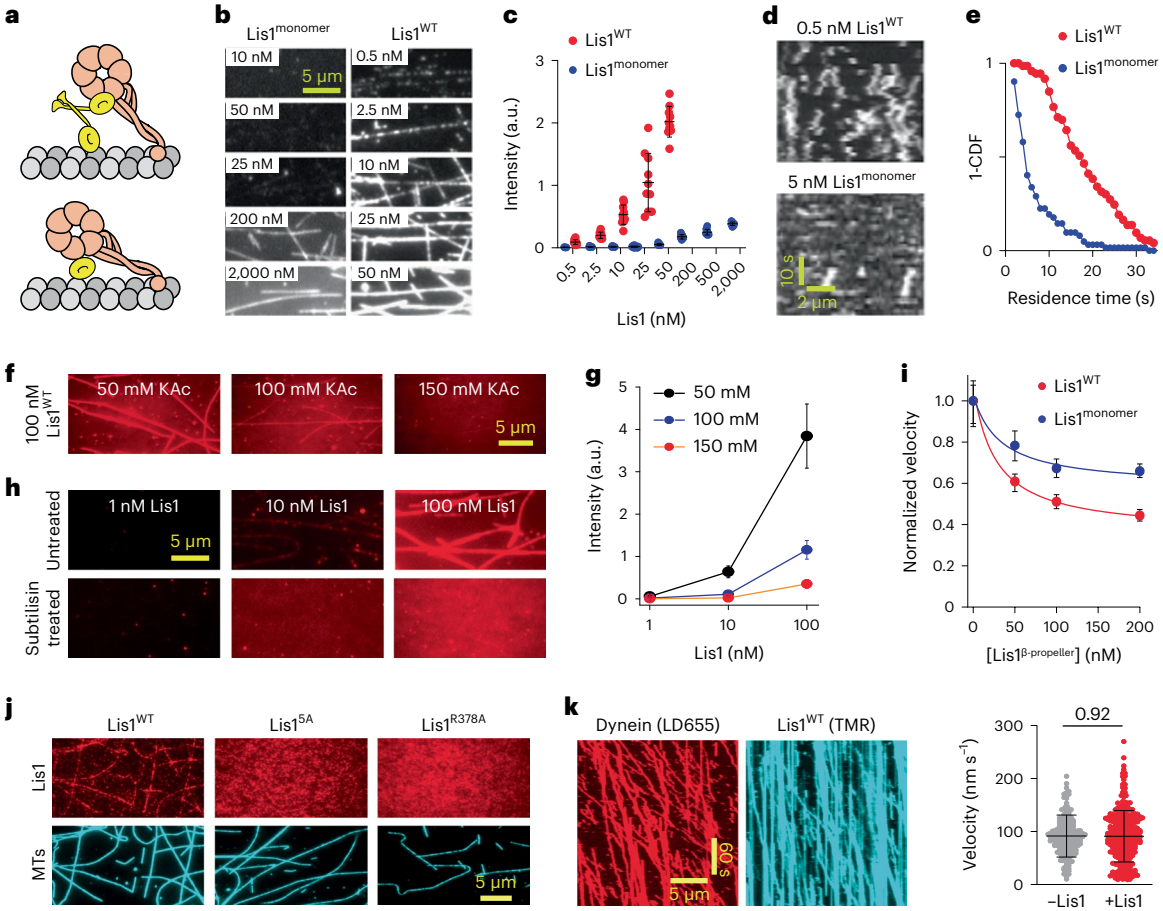

Fig. 2 | Lis1 slows dynein motility in the absence of its interaction with microtubules. a, Models of dynein tethered to a microtubule either via one Lis1 β-propeller docked to dynein and the other on the microtubule (top) or one Lis1 β-propeller simultaneously interacting with dynein and the microtubule (bottom). **b**, Representative images of different concentrations of LD655-labeled $Lis1^{WT}$ and $Lis1^{monomer}$ binding to microtubules. **c**, Fluorescence intensities of $Lis1^{WT}$ and $Lis1^{monomer}$ on microtubules (mean ± s.d.; $n = 10$ microtubules per condition; three technical replicates). **d**, Kymographs show landing, diffusion and dissociation of $Lis1^{WT}$ and $Lis1^{monomer}$ from microtubules. **e**, The inverse cumulative distribution function (1-CDF) of the microtubule residence time of $Lis1^{WT}$ and $Lis1^{monomer}$ ($n = 73$ for $Lis1^{WT}$ and 62 for $Lis1^{monomer}$). **f**, $Lis1^{WT}$ binding to microtubules is reduced by salt (three independent experiments). **g**, The average intensity of $Lis1^{WT}$ on microtubules in different salt concentrations (mean ± s.d.; $n = 10$ microtubules per condition; three technical replicates). **h**, $Lis1^{WT}$ does not decorate subtilisin-treated microtubules in 50 mM KAc. **i**, Normalized velocity of dynein with increasing concentrations of $Lis1^{WT}$ or $Lis1^{monomer}$. The median and interquartile ranges are shown ($n = 400$ runs per condition). Solid curves represent a fit to reveal the K_d (28 nM for $Lis1^{WT}$ and 35 nM for $Lis1^{monomer}$) and the minimum value for the normalized velocity (0.36 for $Lis1^{WT}$ and 0.58 for $Lis1^{monomer}$). **j**, Unlike $Lis1^{WT}$, $Lis1^{5A}$ and $Lis1^{R378A}$ do not bind microtubules (three independent experiments). Lis1 concentration was set to 100 nM and the assays were performed in 50 mM KAc. MTs, microtubules. **k**, A representative kymograph of dynein motility on Lis1-decorated microtubules. Occasionally, dynein picks up Lis1 on microtubules and comigrates with it during processive motility. Lis1 trajectories without comigrating dynein are due to incomplete labeling of the motor (left). Velocities of dynein motors on undecorated (−Lis1) and Lis1-decorated (+Lis1) microtubules ($n = 208$ and 329, from left to right) (right). The P value was calculated by a two-tailed t-test with Welch correction. In **c** and **k**, the center line and whiskers represent the mean and s.d., respectively.

Because all dyneins would encounter microtubule-bound Lis1, this model predicts a similar reduction in velocity for dyneins that comigrate with Lis1 and those that are not bound to Lis1 (ref. 20). To test this model, we predecorated microtubules with 300 nM Lis1 with no added salt and washed away free Lis1 from the chamber (Extended Data Fig. 2f). We found that 92% of Lis1 intensity disappeared after washing the chamber and introducing dynein, consistent with transient and diffusive interactions of Lis1 with the microtubule. The fraction of Lis1 remaining on the microtubules failed to impede dynein motility (Fig. 2k and Supplementary Videos 3 and 4), indicating that Lis1 does not serve as an effective roadblock on the microtubule against dynein motility.

We also purified dynein from the *S. cerevisiae* strain that overexpresses DHC and each of its associated chains under the galactose promoter (hereafter $dynein_{Gal}$) to explore why this construct exhibits slower motility in the presence of Lis1 even when it is not directly bound to Lis1[20]. Similar to dynein expressed using the endogenous promoter (Fig. 1), $dynein_{Gal}$ had an increased run time when colocalized with Lis1 (Extended Data Figs. 3 and 4). However, $dynein_{Gal}$ motors moved substantially slower whether or not they colocalized with Lis1 in the chamber (Extended Data Fig. 4d,f), as reported[20]. The reduction in $dynein_{Gal}$ velocity was not due to the decoration of the microtubule surface by Lis1, because Lis1 addition slowed $dynein_{Gal}$ even when it did not efficiently decorate microtubules under physiological salt (150 mM; Extended Data Fig. 3). We next introduced or removed Lis1 from the chamber while recording $dynein_{Gal}$ motility. Introducing Lis1 into the chamber did not alter the velocity of $dynein_{Gal}$ motors that were already moving along the microtubule at the time Lis1 was added (Extended Data Fig. 5a–c). Likewise, the removal of free Lis1 from the chamber failed to recover $dynein_{Gal}$ velocity (Extended Data Fig. 5c), indicating that $dynein_{Gal}$ velocity is reduced when it is preincubated with Lis1, not by the comigration of Lis1 on the microtubule. While the

https://doi.org/10.1038/s41589-023-01464-6

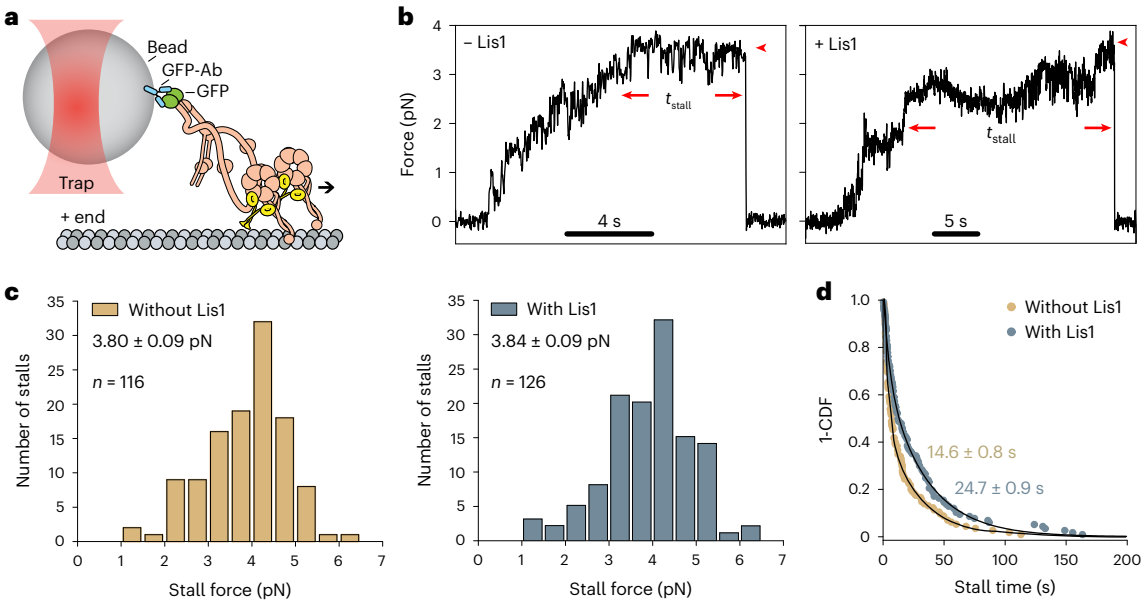

Fig. 3 | Lis1 does not affect the stall force of dynein. a, The schematic shows stall force measurements of GFP-dynein in the presence of unlabeled Lis1 using a fixed-beam optical trap. Ab, antibody. **b**, Sample trajectories of beads driven by single dynein motors in 1 mM ATP with and without 300 nM Lis1. The arrowheads indicate the detachment of the motor from the microtubule and the snapping of the bead to the trap center. The arrows show the beginning and the end of a stalling event. Stall time (t_{stall}) was defined as the time the bead spends at the 30% margin of the stall force before it detaches from the microtubule. **c**, The stall force histogram of dynein in the presence and absence of 300 nM Lis1 (mean ± s.e.m.; $P = 0.77$, two-tailed t-test). **d**, Stall times of dynein with and without 300 nM Lis1. Fit to a double exponential decay (solid curves) reveals the weighted average of t_{stall} (±s.e.).

underlying mechanism remains unclear, the differences between the Lis1-mediated regulation of dynein and dynein$_{Gal}$ may be related to low stability or aggregation of dynein$_{Gal}$ after purification[20] (see 'Protein purification and labeling' in Methods).

Lis1 does not affect the dynein stall force

We next investigated whether Lis1 binding slows dynein motility by interfering with the swinging motion of the linker at the surface of the ring[25]. Because the linker drives the force-generating powerstroke of dynein, this model predicts that Lis1 binding reduces the ability of dynein to walk against hindering forces. To test this possibility, we measured the stall force of endogenously expressed dynein in the presence and absence of excess (300 nM) Lis1 using an optical trap (Fig. 3a). In the absence of Lis1, dynein stalled at 3.8 ± 0.1 pN (mean ± s.e.m., $n = 116$ stalls) and remained attached to the microtubule for 14.6 ± 0. 8 s (mean ± s.e.m.) before the trapped bead snapped back to the trap center[34] (Fig. 3b,c). The stall force was unaltered by Lis1 addition (3.8 ± 0.1 pN, $n = 126$ stalls; Fig. 3b,c), suggesting that Lis1 does not disrupt the force-generating powerstroke of the linker. However, the Lis1 addition resulted in a 70% increase in the duration of the stalls (24.7 ± 0.9 s, $P = 0.018$, two-tailed Kolmogorov–Smirnov test), indicating that Lis1 reduces the microtubule detachment rate of dynein under hindering forces (Fig. 3d)[18,36].

Unlike full-length dynein, Lis1 binding reduced the stall force of tail-truncated and artificially dimerized dynein constructs[34,40], suggesting that artificial dimerization of the linkers at the exit of the ring introduces a steric obstacle against their swinging motion when Lis1 is present on the outer surface of the ring (Extended Data Fig. 6). However, Lis1 binding does not affect the force generation of full-length dynein, presumably because the longer length of the full-length dynein tails has greater flexibility compared to the truncated dynein constructs[25].

Lis1 slows force-induced detachment of dynein

Because Lis1 increases the microtubule affinity of dynein (Fig. 1)[17,22,23,25], we also tested whether Lis1 binding slows motility by altering the detachment kinetics of dynein from the microtubule. Dynein controls its microtubule affinity by altering the registry of the stalk coiled coils through nucleotide-dependent conformational changes in the AAA+ ring[5]. The stalk sliding mechanism is also sensitive to external forces[41]. When pulled in the assisting direction (towards the minus end of microtubules), the stalk switches to a weak binding registry, and dynein releases quickly from the microtubule and moves substantially faster. However, the stalk remains in a strongly bound registry and the motor resists backward movement when pulled in the hindering direction[34,41–44].

If Lis1 binding interferes with the stalk sliding mechanism, we anticipated the addition of Lis1 to alter the force–velocity (F–V) behavior of dynein. To test this prediction, we first measured the velocity of single dynein motors in 1 mM ATP and in the absence of Lis1 when they were subjected to constant forces in assisting and hindering directions using a force-feedback controlled trap. Consistent with previous reports[34,40,44], hindering force slowed minus end-directed motility of dynein and the motors start walking towards the plus end under super-stall forces. In comparison, the minus end-directed velocity of dynein motility increased more rapidly under the same magnitude forces in the assisting direction (Fig. 4a). The addition of 300 nM Lis1 reduced dynein speed when the motor was being pulled in either direction (Fig. 4b), but the speed was reduced more substantially under assisting forces than under hindering forces (Fig. 4c,d). To quantify the changes in the asymmetry in F–V of dynein, we compared the speed of the motor when it walks towards the plus end versus the minus end of the microtubule under force. Because dynein changes its direction relative to the stall force, not by the actual direction of the applied force, in the presence of ATP[34,40], we defined the asymmetry as the ratio of forward and backward speeds of dynein when the motor is subjected to the same magnitude of forces relative to the stall force (F_{rel}). Consistent with our hypothesis, Lis1 addition substantially reduced the asymmetry between plus end- and minus end-directed speeds of dynein from 2.45 to 1.14, on average (Fig. 4c,d).

We reasoned that Lis1 binding may reduce the asymmetry in F–V by interfering with either the linker swing or the stalk sliding mechanisms

https://doi.org/10.1038/s41589-023-01464-6

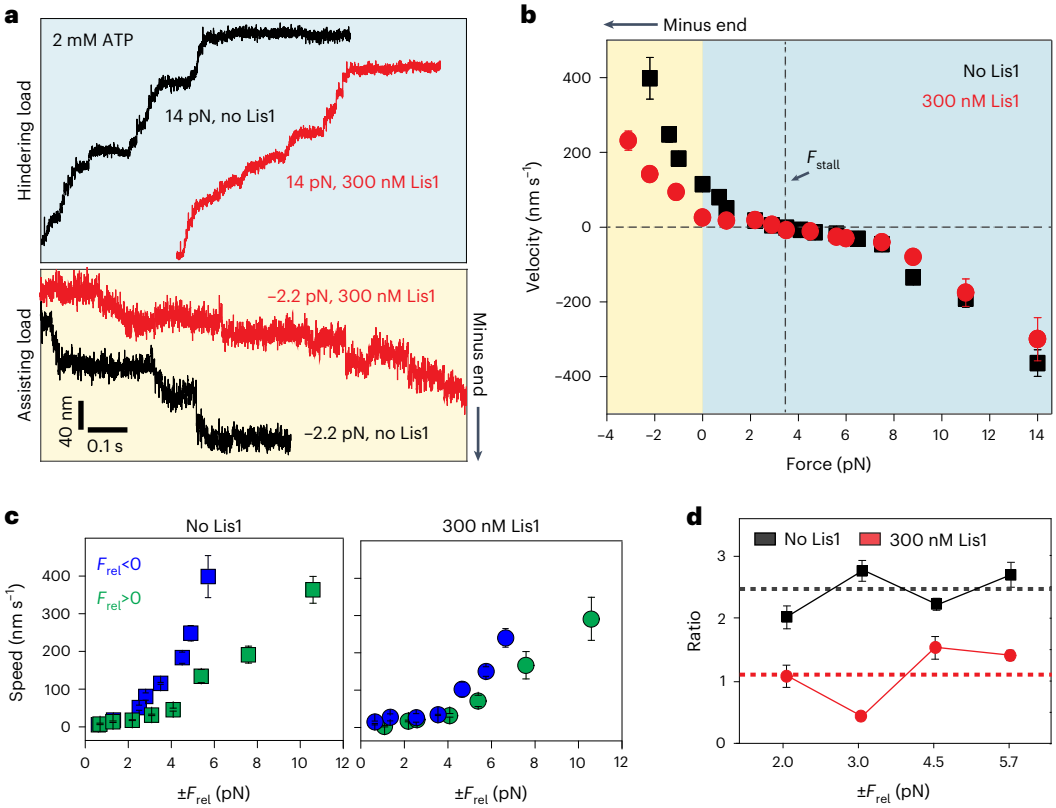

Fig. 4 | Lis1 reduces the asymmetry in the *F*–*V* behavior of dynein in the presence of ATP. a, Representative traces of dynein-driven beads under hindering (positive) and assisting (negative) forces with and without 300 nM Lis1. Assays were performed in 2 mM ATP and 50 mM KAc. **b**, *F*–*V* measurements of dynein in the presence and absence of 300 nM Lis1 (mean ± s.e.m.; from left to right, n = 41, 38, 37, 861, 27, 52, 106, 28, 51, 60, 89, 115, 124, 62, 23, 38 and 40 runs without Lis1 and 34, 52, 25, 312, 33, 42, 49, 37, 62, 47, 33, 42, 36, 29 and 18 runs with Lis1). Dashed lines represent the force at which the average motor velocity is 0 (F_{stall}). **c**, The speed of dynein-driven beads under the same magnitude of positive and negative forces relative to the stall force (F_{rel}; mean ± s.e.m.; from left to right, n = 51, 28, 106, 52, 27, 861, 37, 38 and 41 runs for F_{rel} < 0 and 60, 89, 115, 124, 62, 23, 38 and 40 runs for F_{rel} > 0 without Lis1 and 49, 42, 33, 312, 25, 52 and 34 runs for F_{rel} < 0 and 37, 62, 47, 33, 42, 36, 29 and 18 runs for F_{rel} > 0 with 300 nM Lis1). **d**, The asymmetry ratios of the dynein speeds under the same magnitude of positive and negative F_{rel}. The dashed lines represent the average of the asymmetry ratios measured under different forces. The error bars represent s.e.m.

of dynein. The swinging motion of the linker is strictly coupled to the nucleotide-dependent rigid-body motions of the AAA+ ring[45], whereas the registry of the stalk coiled coils can be altered by external force even in the absence of ATP[41]. To distinguish between these possibilities, we tested whether Lis1 still affects the asymmetry in the *F*–*V* of dynein in the absence of ATP. Similar to the ATP condition, we observed Lis1 addition to decrease dynein speed when the motor was pulled in both directions, and the decrease in speed was more substantial when the motor was pulled in the assisting direction in the absence of ATP (Fig. 5a,b). Because the motor moves in a direction that it is pulled in the absence of ATP, we calculated the asymmetry relative to the no-force condition in this case. Lis1 addition reduced the asymmetry from 1.83 to 1.10, on average (Fig. 5c). These results indicate that Lis1 binding slows the detachment of dynein from microtubules by interfering with the stalk sliding mechanism, not by interfering with the swinging motion of the linker.

We previously showed that Lis1 stably interacts with a second binding site at the base of the dynein stalk[16,46]. To test whether this Lis1–stalk interaction might be responsible for the ability of Lis1 to reduce the asymmetry in force-induced detachment of dynein from microtubules, we performed *F*–*V* measurements using a dynein mutant, in which three Lis1-interacting residues on its stalk were replaced with alanine (dynein^{EQN}, purified from yeast endogenously expressing dynein subunits)[16]. We first confirmed that dynein^{EQN} motility is slowed down by Lis1, albeit with an approximately three-fold higher K_d (54 ±10 nM, ±s.e.) compared to that for wild-type (WT) dynein[16] (Extended Data Fig. 7a,b). Similar to WT dynein, the binding of two Lis1 dimers further slowed dynein^{EQN} motility (Extended Data Fig. 7c,d). In the absence of Lis1, dynein^{EQN} also had a similar stall force, but lower stall times relative to WT dynein (P = 0.03, two-tailed Kolmogorov–Smirnov test; Extended Data Fig. 7e–g). To determine how Lis1 affects stall force and the *F*–*V* behavior of dynein^{EQN}, we used higher concentrations of Lis1 (900 nM) to compensate for the lower affinity of dynein^{EQN} for Lis1 (ref. 16). The addition of Lis1 resulted in only minor changes in the stall force and stall time of dynein^{EQN} (Extended Data Fig. 7e–g). However, unlike WT dynein, the addition of Lis1 did not reduce the asymmetry of the *F*–*V* behavior of dynein^{EQN} (2.1 without Lis1 and 2.0 with Lis1; Fig. 6 and Extended Data Fig. 8). Collectively, these results show that the Lis1–stalk interaction increases the affinity of Lis1 to bind dynein and reduces the asymmetry in force-induced detachment of dynein from the microtubule, but the Lis1–ring interaction is sufficient to increase the microtubule affinity and reduce the velocity of dynein.

Discussion

In this study, we used single-molecule imaging to test the models that describe how Lis1 affects the motility of yeast cytoplasmic dynein. Because yeast dynein walks processively in the absence of dynactin and an activating adaptor in vitro, we were able to investigate how Lis1 binding affects the inherent motility and force-generation properties of single dynein motors. We observed that when dynein colocalizes with one or two Lis1 dimers, it moves more slowly and runs on

https://doi.org/10.1038/s41589-023-01464-6

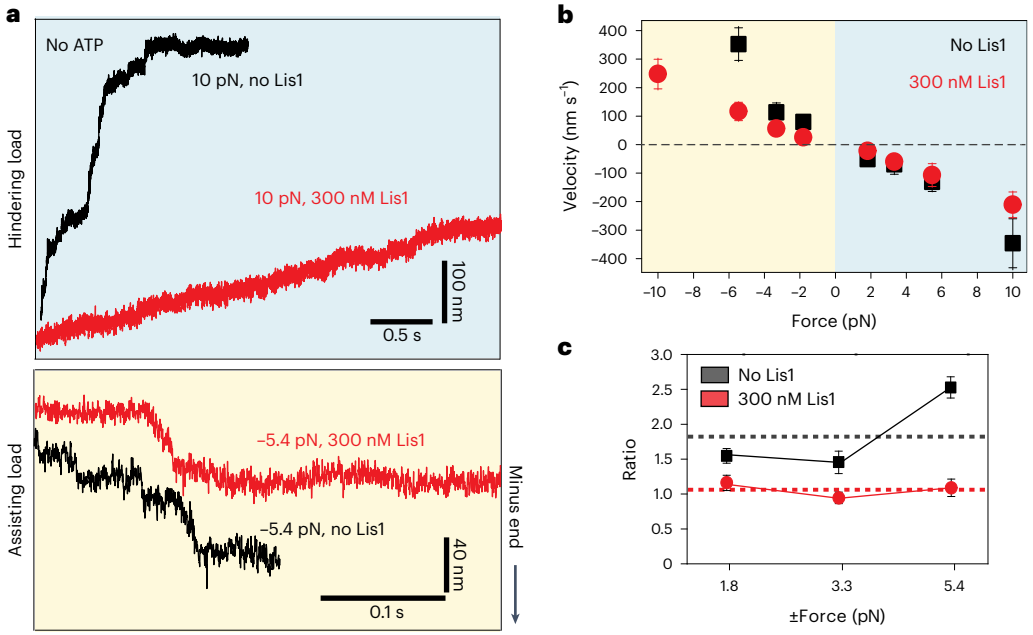

Fig. 5 | Lis1 reduces the asymmetry in *F*–*V* of dynein in the absence of ATP. **a**, Representative traces of dynein-driven beads under assisting and hindering forces with and without 300 nM Lis1. Assays were performed in 50 mM KAc and without ATP. **b**, *F*–*V* measurements of dynein in the absence and presence of 300 nM Lis1 (mean ± s.e.m.; from left to right, n = 42, 29, 65, 51, 38, 62 and 15 runs without Lis1 and 36, 35, 34, 28, 21, 25, 20 and 19 runs with Lis1). **c**, The ratios of the velocities under the same magnitude of forces in assisting and hindering directions relative to 0 pN force. The dashed lines represent the average of the asymmetry ratios measured under different forces. The error bars represent s.e.m.

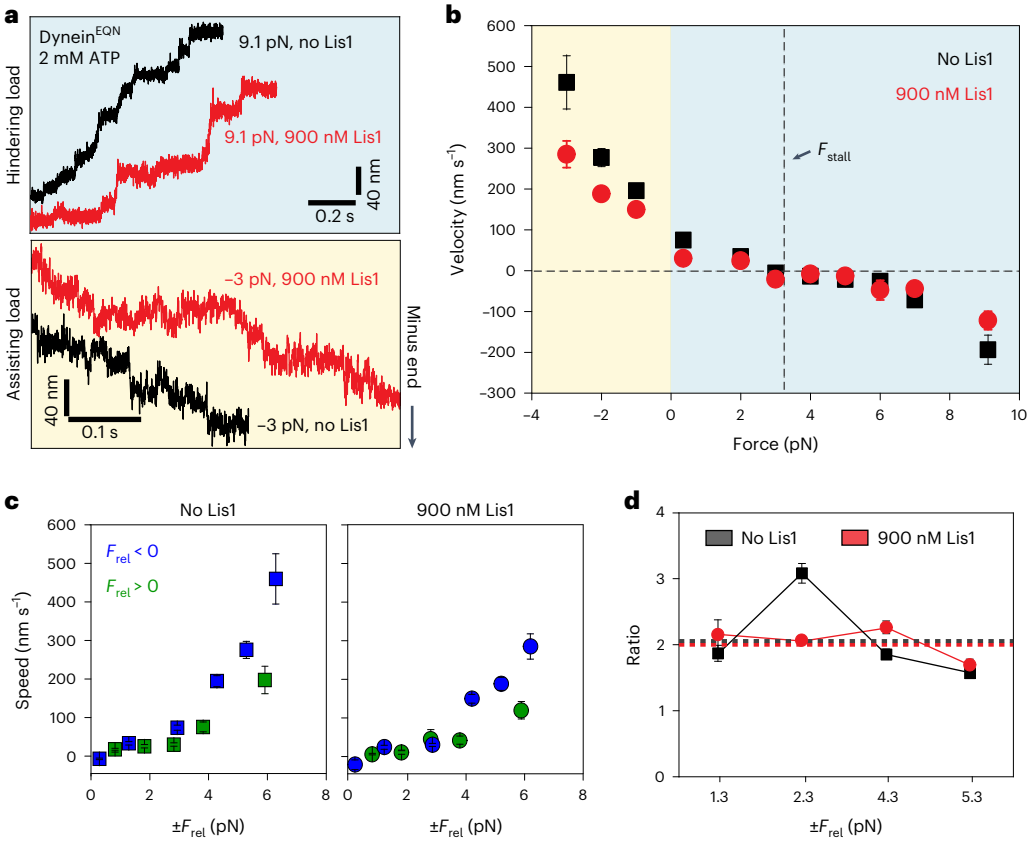

Fig. 6 | Mutagenesis of the Lis1-binding site on the dynein stalk recovers the asymmetry in *F*–*V* of dynein. **a**, Representative traces of dynein^{EQN}-driven beads under assisting and hindering forces with and without 900 nM Lis1. Assays were performed in 2 mM ATP and 50 mM KAc. **b**, *F*–*V* measurements of dynein^{EQN} with and without 900 nM Lis1 (mean ± s.e.m.; from left to right, n = 31, 66, 62, 48, 47, 26, 42, 39, 23, 45 and 33 runs without Lis1 and 54, 36, 61, 31, 37, 17, 54, 14, 19, 38 and 26 runs with Lis1). **c**, The speed of dynein^{EQN}-driven beads under the same magnitude of positive and negative forces relative to the stall force of dynein^{EQN} (3.3 pN; mean ± s.e.m.; from left to right, n = 26, 47, 48, 62, 66 and 31 runs for F_{rel} < 0 and 42, 39, 23, 45 and 33 runs for F_{rel} > 0 without Lis1 and 17, 37, 31, 61, 36 and 54 runs for F_{rel} < 0 and 54, 14, 19, 38 and 26 runs for F_{rel} > 0 with 900 nM Lis1). **d**, The ratios of the velocities under the same magnitude of forces relative to the stall force. The dashed lines represent the average of the asymmetry ratios measured under different forces. The error bars represent s.e.m.

microtubules for a longer time than motors that do not colocalize with Lis1. We conclude that Lis1 binding to dynein is necessary to induce increased microtubule affinity and decreased velocity. These results are consistent with our previous observations that Lis1 binding slows the motility of yeast dynein[16,17] as well as mammalian dynein–dynactin[18,19], and inconsistent with reports that Lis1 colocalization increases[26] or does not change[27] the speed of mammalian dynein–dynactin. This discrepancy may be relevant to the two competing effects of Lis1 on the velocity of mammalian dynein–dynactin: Lis1 mediates the assembly of faster complexes that recruit two dyneins to dynactin, but it slows the motility of active complexes if it remains bound to dynein[18,19]. Therefore, the overall effect of Lis1 on mammalian dynein–dynactin might depend on the stoichiometry of Lis1 and dynein in the complex.

We observed that Lis1 weakly interacts with the C-terminal tails of tubulin at low salt[20] through the same surface of its β-propeller domain that interacts with dynein. Although its microtubule-binding affinity is reduced by nearly two orders of magnitude, Lis1 still effectively slows dynein motility at physiological salt concentrations[20]. In addition, dynein motility can be slowed by a single Lis1 β-propeller domain[17], which cannot simultaneously interact with dynein and the microtubule. Collectively, our results are inconsistent with a model that Lis1 slows dynein motility by tethering the motor to the microtubule[20] and show that Lis1 still slows dynein motility under conditions in which it does not interact with the microtubule. Lis1 is also unlikely to serve as an effective roadblock against dynein motility because it exhibits diffusive motion on microtubules and its microtubule decoration does not substantially affect dynein motility along these tracks.

We also performed optical trapping assays to determine how Lis1 binding affects force generation and the force response of dynein. Similar to mammalian dynein[18], Lis1 binding does not affect the stall force of yeast dynein, indicating that the linker can perform its force-generating powerstroke when Lis1 is bound to the AAA+ ring. This result is consistent with the ability of dynein motors to walk processively, albeit at lower speeds, when colocalized with Lis1 (refs. 18,19), whereas disrupting the linker swing mechanism fully abrogates the motility[47]. Lis1-bound dynein also persists against microtubule detachment for longer durations under hindering forces and moves slower under both assisting and hindering forces, consistent with the high microtubule affinity of Lis1-bound dynein[17,22,23,25]. These results are consistent with previous studies that reported an increase in stall duration of isolated mammalian dynein or the mammalian dynein–dynactin–adaptor complex in the presence of Lis1 (refs. 18,36), underscoring the conservation of Lis1 function across evolution.

Based on our results and previous reports, we propose that Lis1 slows dynein motility in two distinct steps. First, Lis1 binding to the AAA+ ring traps the ring in a conformation that favors high microtubule affinity[16]. Because Lis1 still slows the motility of dynein^{EQN} in the absence of force, Lis1 binding to the AAA+ ring is sufficient for slower movement[15,16]. Second, Lis1 binding to the stalk traps the coiled coils in a strongly bound registry and restricts their registry shift. In the absence of Lis1, the stalk can switch from the strongly bound to the weakly bound registry when dynein is subjected to assisting forces, but remains in a strongly bound registry under hindering forces[41]. Lis1 binding slows dynein speed in both assisting and hindering forces, but it has a more profound effect in limiting the acceleration of dynein under assisting forces. We suggest that this is because Lis1 binding to the stalk of dynein prevents the shift of the coiled coils to a registry with lower microtubule affinity by an external force. Consistent with this model, Lis1 is less effective in reducing dynein speed under assisting forces when the stalk residues that interact with Lis1 are mutated to alanine.

Our results are consistent with the role of Lis1 in relieving the autoinhibition of dynein in the phi conformation and facilitating the assembly of the dynein–dynactin complex[18–21]. In vivo studies suggest that Lis1 has additional regulatory roles in addition to rescuing dynein from its autoinhibited conformation, because mutations that disrupt the phi conformation of dynein do not fully rescue loss of endogenous Lis1 (refs. 20,21). Lis1 binding not only opens the phi conformation, but also induces tight microtubule binding of open dynein[36]. This may contribute to the assembly of dynein with dynactin and an activating adaptor by recruiting the motor to the site of assembly and preventing its premature detachment from the microtubule.

Lis1 has been reported to be absent from moving dynein cargos in vivo[48–50] and it appears to dissociate from most dynein complexes during or after the activation of processive motility in vitro[18–20,51–53]. Dissociation of Lis1 may be a key step in dynein activation because enhancing the affinity of dynein for Lis1 leads to defects in nuclear migration in *S. cerevisiae*[37]. However, Lis1 may remain bound to dynein when it transports high-load cargos or pulls on astral microtubules during cell division[54,55]. Lis1 binding may prevent microtubule detachment of dynein when the motor is subjected to both assisting and hindering forces during back-and-forth oscillations of spindle microtubules, thereby enabling multiple dyneins to effectively increase tension for proper positioning of the spindle. Future studies are required to determine whether the association and dissociation of Lis1 from dynein are regulated in different cellular contexts.

Online content

Any methods, additional references, Nature Portfolio reporting summaries, source data, extended data, supplementary information, acknowledgements, peer review information; details of author contributions and competing interests; and statements of data and code availability are available at https://doi.org/10.1038/s41589-023-01464-6.

References

1. Canty, J. T., Tan, R., Kusakci, E., Fernandes, J. & Yildiz, A. Structure and mechanics of dynein motors. *Annu. Rev. Biophys.* **50**, 549–574 (2021).
2. Reck-Peterson, S. L., Redwine, W. B., Vale, R. D. & Carter, A. P. The cytoplasmic dynein transport machinery and its many cargoes. *Nat. Rev. Mol. Cell Biol.* **19**, 382–398 (2018).
3. Guedes-Dias, P. & Holzbaur, E. L. F. Axonal transport: driving synaptic function. *Science* **366**, eaaw9997 (2019).
4. Carter, A. P., Cho, C., Jin, L. & Vale, R. D. Crystal structure of the dynein motor domain. *Science* **331**, 1159–1165 (2011).
5. Kon, T. et al. The 2.8 Å crystal structure of the dynein motor domain. *Nature* **484**, 345–350 (2012).
6. Can, S., Lacey, S., Gur, M., Carter, A. P. & Yildiz, A. Directionality of dynein is controlled by the angle and length of its stalk. *Nature* **566**, 407–410 (2019).
7. Kon, T. et al. Helix sliding in the stalk coiled coil of dynein couples ATPase and microtubule binding. *Nat. Struct. Mol. Biol.* **16**, 325–333 (2009).
8. Torisawa, T. et al. Autoinhibition and cooperative activation mechanisms of cytoplasmic dynein. *Nat. Cell Biol.* **16**, 1118–1124 (2014).
9. Trokter, M., Mucke, N. & Surrey, T. Reconstitution of the human cytoplasmic dynein complex. *Proc. Natl Acad. Sci. USA* **109**, 20895–20900 (2012).
10. Zhang, K. et al. Cryo-EM reveals how human cytoplasmic dynein is auto-inhibited and activated. *Cell* **169**, 1303–1314.e18 (2017).
11. McKenney, R. J., Huynh, W., Tanenbaum, M. E., Bhabha, G. & Vale, R. D. Activation of cytoplasmic dynein motility by dynactin-cargo adapter complexes. *Science* **345**, 337–341 (2014).
12. Schlager, M. A., Hoang, H. T., Urnavicius, L., Bullock, S. L. & Carter, A. P. In vitro reconstitution of a highly processive recombinant human dynein complex. *EMBO J.* **33**, 1855–1868 (2014).
13. Markus, S. M., Marzo, M. G. & McKenney, R. J. New insights into the mechanism of dynein motor regulation by lissencephaly-1. *eLife* **9**, 59737 (2020).

14. Reiner, O. et al. Isolation of a Miller–Dieker lissencephaly gene containing G protein β-subunit-like repeats. *Nature* **364**, 717–721 (1993).
15. Gillies, J. P. et al. Structural basis for cytoplasmic dynein-1 regulation by Lis1. *eLife* **11**, 71229 (2022).
16. DeSantis, M. E. et al. Lis1 has two opposing modes of regulating cytoplasmic dynein. *Cell* **170**, 1197–1208.e12 (2017).
17. Huang, J., Roberts, A. J., Leschziner, A. E. & Reck-Peterson, S. L. Lis1 acts as a 'clutch' between the ATPase and microtubule-binding domains of the dynein motor. *Cell* **150**, 975–986 (2012).
18. Elshenawy, M. M. et al. Lis1 activates dynein motility by modulating its pairing with dynactin. *Nat. Cell Biol.* **22**, 570–578 (2020).
19. Htet, Z. M. et al. LIS1 promotes the formation of activated cytoplasmic dynein-1 complexes. *Nat. Cell Biol.* **22**, 518–525 (2020).
20. Marzo, M. G., Griswold, J. M. & Markus, S. M. Pac1/LIS1 stabilizes an uninhibited conformation of dynein to coordinate its localization and activity. *Nat. Cell Biol.* **22**, 559–569 (2020).
21. Qiu, R., Zhang, J. & Xiang, X. LIS1 regulates cargo-adapter-mediated activation of dynein by overcoming its autoinhibition in vivo. *J. Cell Biol.* **218**, 3630–3646 (2019).
22. Yamada, M. et al. LIS1 and NDEL1 coordinate the plus-end-directed transport of cytoplasmic dynein. *EMBO J.* **27**, 2471–2483 (2008).
23. Torisawa, T. et al. Functional dissection of LIS1 and NDEL1 towards understanding the molecular mechanisms of cytoplasmic dynein regulation. *J. Biol. Chem.* **286**, 1959–1965 (2011).
24. Wang, S. et al. Nudel/NudE and Lis1 promote dynein and dynactin interaction in the context of spindle morphogenesis. *Mol. Biol. Cell* **24**, 3522–3533 (2013).
25. Toropova, K. et al. Lis1 regulates dynein by sterically blocking its mechanochemical cycle. *eLife* **3**, 03372 (2014).
26. Baumbach, J. et al. Lissencephaly-1 is a context-dependent regulator of the human dynein complex. *eLife* **6**, 21768 (2017).
27. Gutierrez, P. A., Ackermann, B. E., Vershinin, M. & McKenney, R. J. Differential effects of the dynein-regulatory factor Lissencephaly-1 on processive dynein-dynactin motility. *J. Biol. Chem.* **292**, 12245–12255 (2017).
28. Muhua, L., Karpova, T. S. & Cooper, J. A. A yeast actin-related protein homologous to that in vertebrate dynactin complex is important for spindle orientation and nuclear migration. *Cell* **78**, 669–679 (1994).
29. Heil-Chapdelaine, R. A., Oberle, J. R. & Cooper, J. A. The cortical protein Num1p is essential for dynein-dependent interactions of microtubules with the cortex. *J. Cell Biol.* **151**, 1337–1344 (2000).
30. Reck-Peterson, S. L. et al. Single-molecule analysis of dynein processivity and stepping behavior. *Cell* **126**, 335–348 (2006).
31. DeWitt, M. A., Chang, A. Y., Combs, P. A. & Yildiz, A. Cytoplasmic dynein moves through uncoordinated stepping of the AAA+ ring domains. *Science* **335**, 221–225 (2012).
32. Qiu, W. et al. Dynein achieves processive motion using both stochastic and coordinated stepping. *Nat. Struct. Mol. Biol.* **19**, 193–200 (2012).
33. Belyy, V. et al. The mammalian dynein-dynactin complex is a strong opponent to kinesin in a tug-of-war competition. *Nat. Cell Biol.* **18**, 1018–1024 (2016).
34. Belyy, V., Hendel, N. L., Chien, A. & Yildiz, A. Cytoplasmic dynein transports cargos via load-sharing between the heads. *Nat. Commun.* **5**, 5544 (2014).
35. Elshenawy, M. M. et al. Cargo adaptors regulate stepping and force generation of mammalian dynein-dynactin. *Nat. Chem. Biol.* **15**, 1093–1101 (2019).
36. McKenney, R. J., Vershinin, M., Kunwar, A., Vallee, R. B. & Gross, S. P. LIS1 and NudE induce a persistent dynein force-producing state. *Cell* **141**, 304–314 (2010).
37. Markus, S. M. & Lee, W. L. Regulated offloading of cytoplasmic dynein from microtubule plus ends to the cortex. *Dev. Cell* **20**, 639–651 (2011).
38. Monroy, B. Y. et al. A combinatorial MAP code dictates polarized microtubule transport. *Dev. Cell* **53**, 60–72.e4 (2020).
39. Ferro, L. S. et al. Structural and functional insight into regulation of kinesin-1 by microtubule-associated protein MAP7. *Science* **375**, 326–331 (2022).
40. Gennerich, A., Carter, A. P., Reck-Peterson, S. L. & Vale, R. D. Force-induced bidirectional stepping of cytoplasmic dynein. *Cell* **131**, 952–965 (2007).
41. Rao, L., Berger, F., Nicholas, M. P. & Gennerich, A. Molecular mechanism of cytoplasmic dynein tension sensing. *Nat. Commun.* **10**, 3332 (2019).
42. Cleary, F. B. et al. Tension on the linker gates the ATP-dependent release of dynein from microtubules. *Nat. Commun.* **5**, 4587 (2014).
43. Nicholas, M. P. et al. Cytoplasmic dynein regulates its attachment to microtubules via nucleotide state-switched mechanosensing at multiple AAA domains. *Proc. Natl Acad. Sci. USA* **112**, 6371–6376 (2015).
44. Ezber, Y., Belyy, V., Can, S. & Yildiz, A. Dynein harnesses active fluctuations of microtubules for faster movement. *Nat. Phys.* **16**, 312–316 (2020).
45. Carter, A. P. Crystal clear insights into how the dynein motor moves. *J. Cell Sci.* **126**, 705–713 (2013).
46. Reimer, J. M., DeSantis, M. E., Reck-Peterson, S. L. & Leschziner, A. E. Structures of human dynein in complex with the lissencephaly 1 protein, LIS1. *eLife* **12**, 84302 (2023).
47. Kon, T., Mogami, T., Ohkura, R., Nishiura, M. & Sutoh, K. ATP hydrolysis cycle-dependent tail motions in cytoplasmic dynein. *Nat. Struct. Mol. Biol.* **12**, 513–519 (2005).
48. Lee, W. L., Oberle, J. R. & Cooper, J. A. The role of the lissencephaly protein Pac1 during nuclear migration in budding yeast. *J. Cell Biol.* **160**, 355–364 (2003).
49. Lenz, J. H., Schuchardt, I., Straube, A. & Steinberg, G. A dynein loading zone for retrograde endosome motility at microtubule plus-ends. *EMBO J.* **25**, 2275–2286 (2006).
50. Egan, M. J., Tan, K. & Reck-Peterson, S. L. Lis1 is an initiation factor for dynein-driven organelle transport. *J. Cell Biol.* **197**, 971–982 (2012).
51. Jha, R., Roostalu, J., Cade, N. I., Trokter, M. & Surrey, T. Combinatorial regulation of the balance between dynein microtubule end accumulation and initiation of directed motility. *EMBO J.* **36**, 3387–3404 (2017).
52. Lammers, L. G. & Markus, S. M. The dynein cortical anchor Num1 activates dynein motility by relieving Pac1/LIS1-mediated inhibition. *J. Cell Biol.* **211**, 309–322 (2015).
53. Ton, W. D. et al. Microtubule-binding-induced allostery triggers LIS1 dissociation from dynein prior to cargo transport. *Nat. Struct. Mol. Biol.* **30**, 1365–1379 (2023).
54. Pecreaux, J. et al. Spindle oscillations during asymmetric cell division require a threshold number of active cortical force generators. *Curr. Biol.* **16**, 2111–2122 (2006).
55. Yang, G. et al. Architectural dynamics of the meiotic spindle revealed by single-fluorophore imaging. *Nat. Cell Biol.* **9**, 1233–1242 (2007).

Methods

Protein purification and labeling

The endogenous genomic copies of *S. cerevisiae* dynein heavy chain (*DYN1*) and Lis1 (*PAC1*) were modified or deleted using homologous recombination[30]. The list of strains used in this study is shown in Supplementary Table 1. The strains that express GFP- and Halo-tagged full-length dynein (RPY1732 and 1736) were generated from the parent yeast strains[17,30]. Tagged yeast dynein showed no defects in nuclear segregation, indicating that the dynein promoter is not disrupted in this strain background.

S. cerevisiae strains that express dynein$_{Gal}$ and Lis1 constructs were grown in 2 l YPA-galactose media (1% yeast extract, 1% peptone, 0.004% adenine sulfate, 2% galactose), and strains that express endogenously expressed dynein were grown in 2 l YPD media (1% yeast extract, 1% peptone, 0.004% adenine sulfate, 2% dextrose) until optical density (OD_{600}) reached 2.0. The cells were pelleted at 6,000*g* for 15 min, resuspended in phosphate buffer saline and frozen in liquid nitrogen. For purification of dynein and dynein$_{Gal}$, cell pellets were ground and dissolved in the dynein lysis buffer (DLB; 30 mM HEPES pH 7.4, 2 mM $Mg(Ac)_2$, 1 mM EGTA, 10% glycerol) supplemented with 50 mM KAc, 1 mM DTT, 0.1 mM ATP, 1 mM phenylmethylsulfonyl fluoride (PMSF), 0.1% Triton at 37 °C. The lysate was centrifuged at 360,000*g* for 45 min and the supernatant was incubated with 300 µl IgG beads for 1 h at 4 °C. The mixture was then applied to Qiagen columns, washed with 30 ml DLB supplemented with 250 mM KAc, 1 mM DTT, 0.1 mM ATP, 1 mM PMSF, 0.1% Triton and then with 20 ml TEV buffer (10 mM Tris–HCl pH 8.0, 150 mM KCl, 10% glycerol, 1 mM DTT, 0.1 mM ATP, 0.25 mM PMSF) at 4 °C. The mixture was then incubated with 10 µl of 2 mg ml^{-1} TEV protease for 1 h at 4 °C. The eluted protein was separated from the beads by centrifuging the mixture in Amicon Ultra Free MC tubes at 21,000*g* for 2 min, flash frozen in liquid nitrogen and stored at −80 °C. A similar procedure was used to purify Lis1, except cells were lysed in a Hi-salt phosphate lysis buffer (50 mM potassium phosphate pH 8.0, 150 mM KAc, 2 mM $Mg(Ac)_2$, 10% glycerol, 10 mM imidazole, 150 mM NaCl, 50 mM 2-mercaptoethanol (BME), 1 mM PMSF, 0.2% Triton) and protein was eluted in nu-TEV buffer (50 mM Tris–HCl pH 8.0, 1 mM EGTA, 150 mM KAc, 150 mM NaCl, 2 mM $Mg(Ac)_2$, 10% glycerol, 1 mM DTT, 0.5 mM PMSF). The protein concentration was determined by both 280 nm absorbance and the Bradford assay.

Proteins were labeled with fluorescent dyes after resuspending the lysate with beads and before adding TEV protease. Then, 10 nanomoles of a fluorescent dye were well mixed with the protein–bead mixture and incubated for 1 h at 4 °C. The column was then washed with 100 ml TEV buffer to remove excess dye before eluting the protein from the beads. The labeling percentage was determined by measuring the protein concentration in Bradford assays and the absorbance under 555 nm and 655 nm excitation for TMR/LD555 and Cy5/LD655 dyes, respectively. The probability, p of each SNAP-Lis1 monomer labeled with TMR and LD655 dyes derivatized with benzyl guanine was 0.72 and 0.80 per Lis1 monomer, respectively. The probabilities of a SNAP-Lis1 dimer to be labeled with at least one TMR or LD655 dyes (calculated as $2p - p^2$) were 0.92 and 0.96, respectively. The probability of a dynein dimer being labeled with a dye was 0.8.

Unlike dynein, dynein$_{Gal}$ showed signs of aggregation and slower motility after flash freezing and storage at −80 °C. To avoid the freezing and thawing cycle, dynein$_{Gal}$ experiments were performed immediately after protein preparation.

Microtubule polymerization and subtilisin treatment

Tubulin was purified from pig brains in a 1 M PIPES buffer. Then, 60 ng unlabeled, 60 ng biotinylated and 1 ng fluorescently labeled tubulin were diluted to 1 mg ml^{-1} in 120 µl BRB80 buffer (80 mM PIPES pH 6.8, 2 mM $MgCl_2$, 1 mM EGTA) supplemented with 1× polymerization mixture (1 mM GTP, 10% DMSO) and polymerized at 37 °C for 40 min. The mixture was incubated at 37 °C for an additional 40 min after adding 1 mM taxol. The mixture was centrifuged at 21,000*g* for 13 min at room temperature and resuspended in 30 µl BRB80 buffer supplemented with 10 mM taxol and 1 mM DTT. Microtubules were stored in the dark at room temperature and used within two weeks.

For subtilisin treatment, 2.5 mg ml^{-1} polymerized microtubules were stored in the dark for 1 d for elongation and then incubated with a different concentration of subtilisin for 2 h in a 37 °C bath. Under these conditions, 50 µg ml^{-1} subtilisin cleaved more than 85% of the tubulin tails without substantially affecting dynein motility along these microtubules. The proteolytic cleavage was stopped with the addition of 2 mM PMSF. The microtubules were centrifuged at 21,000*g* for 13 min at room temperature and the pellet was resuspended in BRB80 supplemented with 10 mM taxol.

Single-molecule motility assays

Flow chambers were prepared by placing a multichannel parafilm in between a microscope slide and a cover glass functionalized with PEG/PEG-biotin (Microsurfaces). The chamber was incubated with 20 µl of 2 mg ml^{-1} streptavidin for 2 min and excess streptavidin was removed by washing the chamber with 60 µl dynein motility buffer (DMB; DLB supplemented with 2% pluronic acid, 1 mM taxol, 1 mM tris(2-carboxyethyl) phosphine (TCEP)). The chamber was then incubated with 20 µl of 2 mg ml^{-1} biotinylated microtubules in DMB for 2 min and unbound microtubules were removed by washing the chamber with 80 µl DMB. After 3 min, the chamber was then washed with 20 µl stepping buffer (DLB supplemented with 0.4% pluronic acid, 1 mM taxol, 1 mM TCEP, 2 mM ATP, 1% gloxy (glucose oxidase and catalase), 0.5% dextrose and 50–150 mM KAc). Dynein and Lis1 were diluted in the stepping buffer and incubated on ice for 10 min. A 20 µl motor + Lis1 final mixture in stepping buffer was added to the chamber and the sample was imaged immediately for 15 min.

Lis1–dynein colocalization experiments were performed by mixing fluorescently labeled dynein and Lis1 into the final mixture, before flowing into the chamber. In this assay, colocalization of dynein with a single color of Lis1 might be due to one or two Lis1 dimers bound per dynein, whereas colocalization of both dyes with the GFP signal ensures that two Lis1 dimers are bound to a dynein dimer, one on each motor domain. Colocalization between two differentially labeled dynein was performed by mixing 5 nM LD555-dynein with 5 nM LD655-dynein and leaving on ice for 10 min with or without Lis1. To maximize cross-linking efficiency with different colors of dyneins, dyneins were added to the mixture before Lis1. The dynein–Lis1 mixture was diluted in stepping buffer supplemented with 1 mM ATP and 50 mM KAc.

Single-molecule imaging was performed using a custom-built objective-type multicolor total internal reflection fluorescence (TIRF) microscope equipped with an inverted microscopy body (Nikon Ti-Eclipse), ×100 magnification, 1.49 numerical aperture (NA) plan-apochromat oil immersion objective (Nikon) and a perfect focusing system. The fluorescence signal was detected using an electron-multiplied charge-coupled device (EM-CCD) camera (Andor, Ixon). The effective pixel size after magnification was 108 nm. Samples labeled with GFP, TMR/LD555 and Cy5/LD655 were excited using 0.04 kW cm^{-2} 488, 532 and 633 nm laser beams (Coherent), respectively, and the emission signal was detected using band-pass emission filters (Semrock). For two- and three-color fluorescence assays, imaging was performed using alternating excitation and the time-sharing mode. Single-color videos were recorded at 1 s per frame, whereas multicolor videos were recorded with 0.5 s per frame per color using the time-sharing mode of MicroManager v2.0. To introduce or remove Lis1 from the chamber during imaging, two 0.5 mm diameter holes were drilled on a glass slide at both ends of the flow chamber. The region of interest in the chamber was imaged for 1 min before introducing Lis1 or washing the free Lis1 from the chamber while imaging dynein motility in real time.

Data analysis

Videos were analyzed in ImageJ to create kymographs. Motors that were stationary, exhibited diffusional movement or moved less than 3 pixels were excluded from the analysis. In microtubule residence-time analysis, Lis1 molecules that resided on microtubules for less than 2 frames (2 s) were excluded from the analysis. The results of the data analysis were plotted in Prism and Origin. Data fitting was performed in Origin. 1-CDFs of the run length and run-time data were fitted to a double exponential decay, $y = A_1 e^{-t/\tau_1} + A_2 e^{-t/\tau_2}$, where A_1 and A_2 are the amplitudes and τ_1 and τ_2 are the decay constants. The weighted average of the decay constants, $\tau_{av} = \frac{A_1\tau_1 + A_2\tau_2}{A_1 + A_2}$, was reported as the decay constant[35].

The average velocities of motors that colocalize with 0 (V_0), 1 (V_1) and 2 (V_2) colors of Lis1 were determined from three-color TIRF assays. To determine K_d of Lis1, the average dynein velocity under different Lis1 concentrations, $V([Lis1])$, was fitted to $(1 - p_b)^2 V_0 + 2p_b(1 - p_b)V_1 + (p_b)^2 V_2$, where $p_b = \frac{1}{1 + \frac{K_d}{[Lis1]}}$ is the binding probability of Lis1 to a dynein monomer. The probability of Lis1 colocalization to $dynein_{Gal}$ in Extended Data Fig. 4c was fitted to a binding isotherm function, defined as $C(2p_b - (p_b)^2)$, where C is less than 1 due to incomplete labeling of Lis1 and the limited single-molecule detection ability in the presence of free labeled protein in the flow chamber.

Microtubule copelleting assays

Unlabeled taxol-stabilized microtubules were polymerized as above and free tubulin was removed by centrifugation through a 60% glycerol cushion in BRB80 (80 mM PIPES–KOH pH 6.8, 1 mM $MgCl_2$, 1 mM EGTA, 1 mM DTT, 20 µM taxol) for 15 min at 100,000*g* and 37 °C. The microtubule pellet was resuspended in DLB supplemented with 20 µM taxol. Microtubules (0–600 nM tubulin) were incubated with 100 nM Lis1 for 10 min before being pelleted for 15 min at 100,000*g* and 25 °C. The supernatant was analyzed via SDS–PAGE and depletion was determined using densitometry in ImageJ. Binding curves were fit to a binding isotherm in Origin.

Optical trapping assays

Optical trapping experiments were performed on a custom-built optical trap using a Nikon Ti-E microscope body and a ×100, 1.49 NA plan-apochromat oil immersion objective, as previously described[34]. The beads were trapped with a 2 W 1,064 nm laser (IPG Photonics) and the trap was steered with a two-axis acousto-optical deflector (AA Electronics). The trap stiffness was calculated from the Lorentzian fit to the power spectrum of a trapped bead. For stall force measurements, the trap stiffness was adjusted to allow the motor to walk 100 nm away from the trap center on average before the bead comes to the stall. The position of the bead from the center of the fixed trap was recorded for at least 90 s at 5 kHz.

For fixed trap measurements, 0.8 µm diameter carboxylated latex beads (Life Technologies) were functionalized with 1 mg ml^{-1} rabbit polyclonal GFP antibody (Covance, catalog no. 5314/15), as previously described[34]. In optical trapping assays, 2 mM and 0.25 mM casein was used instead of 2% and 0.4% pluronic acid in DMB and stepping buffer, respectively. The 2 µl of the bead stock were diluted in 8 µl DLB. The 2 µl of diluted beads were sonicated for 8 s. To ensure that more than 90% of the beads are driven by single motors, GFP-dynein was diluted in the stepping buffer to a concentration in which less than 30% of the beads exhibit motility when brought on top of a surface-immobilized axoneme. The mixture was sonicated for 8 s and 2 µl of diluted beads were mixed with 2 µl GFP-dynein, 1.5 µl Lis1 and 2 µl stepping buffer, and incubated on ice for 10 min. For the no Lis1 condition, an equal volume of stepping buffer was added to the mixture instead of Lis1.

Cy5-labeled sea urchin axonemes were nonspecifically adsorbed to the surface of the flow chamber. After 30 s incubation, the chamber was washed with 60 µl DMB to remove the unbound axoneme. After 3 min incubation, the chamber was washed with 60 µl DMB and then with 20 µl stepping buffer. Then, 7.5 µl of the dynein–Lis1 bead mixture was diluted in 20 µl stepping buffer and the KAc concentration was adjusted to 50 mM before being flowed into the chamber. The chamber was sealed with nail polish to prevent evaporation during data acquisition.

Optical trap data were analyzed with a custom-written MATLAB script. The data were downsampled to 500 Hz via median filtering before analysis. Stall events were manually scored when the velocity of the bead movement was reduced to ~0 nm s^{-1} under hindering force and terminated with a sudden (<4 ms) snapping of the bead to the trap center. Events that occurred within a 25 nm distance to the trap center, lasted shorter than 0.4 s or terminated with backward movement, multiple-step detachment or slow (>4 ms) return of the bead to the trap center were excluded from the analysis. Stall forces were calculated as the average force value of the plateau where the bead is nearly immobile before detaching from the axoneme. CDFs of stall times were fitted to a double exponential decay and the weighted average of two decay constants from the fit was reported as the decay constant.

F–*V* measurements

Similar sample preparation procedures were used for *F*–*V* measurements using an optical trap. After the bead movement reached half of the average stall force of the motor, the trapping beam repositioned itself and maintained a 100 nm distance from the bead via a force-feedback mechanism. To determine the microtubule polarity in the no-ATP condition, LD655-labeled GST-Dyn_{331kDA} motors (without a GFP tag) were flowed into the chamber in a stepping buffer supplemented with 30 µM ATP. The motors were allowed to walk on and accumulate at the minus end of surface-immobilized axonemes for 4 mins. The chamber was then washed with 40 µl DMB buffer, followed by 20 µl stepping buffer supplemented with 0.5 U ml^{-1} apyrase instead of ATP to deplete residual ATP in the chamber. The 0.5 U ml^{-1} apyrase was also included in the bead–dynein–Lis1 mixture to remove residual ATP from protein preparations. During optical trapping, microtubule polarity was determined by the minus-end accumulation of the LD655 signal detected by an sCMOS camera (Hamamatsu, Orca Flash v.4.0). Beads were pulled along the length of an axoneme at a constant velocity, and the beads that engaged with the axoneme were trapped by repositioning the trapping beam 100 nm away from the bead center along the direction of the applied force.

The bead position was recorded at 5 kHz and the data were downsampled to 500 Hz via median filtering. The slope of each trace was defined as the velocity of individual motors under an applied force. The traces that were shorter than 70 ms, showed bidirectional motility under force or exhibited instantaneous jumps larger than 50 nm were excluded from data analysis. The asymmetry ratios were calculated by comparing the average velocities under forces equally larger or smaller than F_{stall} in the presence of ATP, and forces equally larger or smaller than 0 pN in the absence of ATP. Velocities at corresponding forces were either directly measured or calculated by linear regression of the measured velocities under the closest force measurements. The errors of asymmetry ratios were determined by error propagation of the compared velocities.

Statistical analysis

The *P* values were calculated by the two-tailed *t*-test for stall force histograms, the two-tailed *t*-test with Welch corrections for velocity measurements and the two-tailed Kolmogorov–Smirnov test for run length and run-time measurements in Prism and Origin. CDFs were calculated in MATLAB.

Reporting summary

Further information on research design is available in the Nature Portfolio Reporting Summary linked to this article.

Data availability

A reporting summary for this article is available as a Supplementary Information file. The main data supporting the findings of this study are available within the article and its Extended Data figures. Protocols that support the findings of this study can be found in Methods. Yeast strains and raw data will be made available by the corresponding authors upon request. Source data are provided with this paper.

Code availability

The custom code used to analyze experimental data is uploaded to the Yildiz Lab code repository (www.yildizlab.org/code_repository) and GitHub (https://github.com/Yildiz-Lab/YFIESTA).

Acknowledgements

We thank S. Can, M. ElShenawy, L. S. Ferro, J. T. Canty and other members of the Yildiz and Reck-Peterson laboratories for helpful discussions, and S. M. Markus for sharing the yeast strain that expresses dynein$_{Gal}$. This work was supported by grants from the National Institute of General Medical Sciences (GM094522, A.Y.), the National Science Foundation (MCB-1617028 and MCB-1055017, A.Y.) and the Fellowship of the Ministry of Education of the Turkish Republic (E.K.). S.L.R.-P. is a Howard Hughes Medical Institute Investigator and is also supported by the National Institutes of Health (1R35GM141825).

Author contributions

E.K., S.L.R.-P. and A.Y. conceived the study and designed the experiments. Z.M.H. generated the yeast constructs for dynein and Lis1. E.K. purified the proteins. E.K. and Y.Z. performed single-molecule experiments and analyzed the data. J.P.G. performed experiments on monomeric Lis1. E.K., S.L.R.-P. and A.Y. wrote the manuscript. All authors read and revised the manuscript.

Competing interests

The authors declare no competing interests.

Additional information

Extended data is available for this paper at https://doi.org/10.1038/s41589-023-01464-6.

Supplementary information The online version contains supplementary material available at https://doi.org/10.1038/s41589-023-01464-6.

Correspondence and requests for materials should be addressed to Ahmet Yildiz.

Peer review information *Nature Chemical Biology* thanks Richard McKenney and the other, anonymous, reviewer(s) for their contribution to the peer review of this work.

https://doi.org/10.1038/s41589-023-01464-6

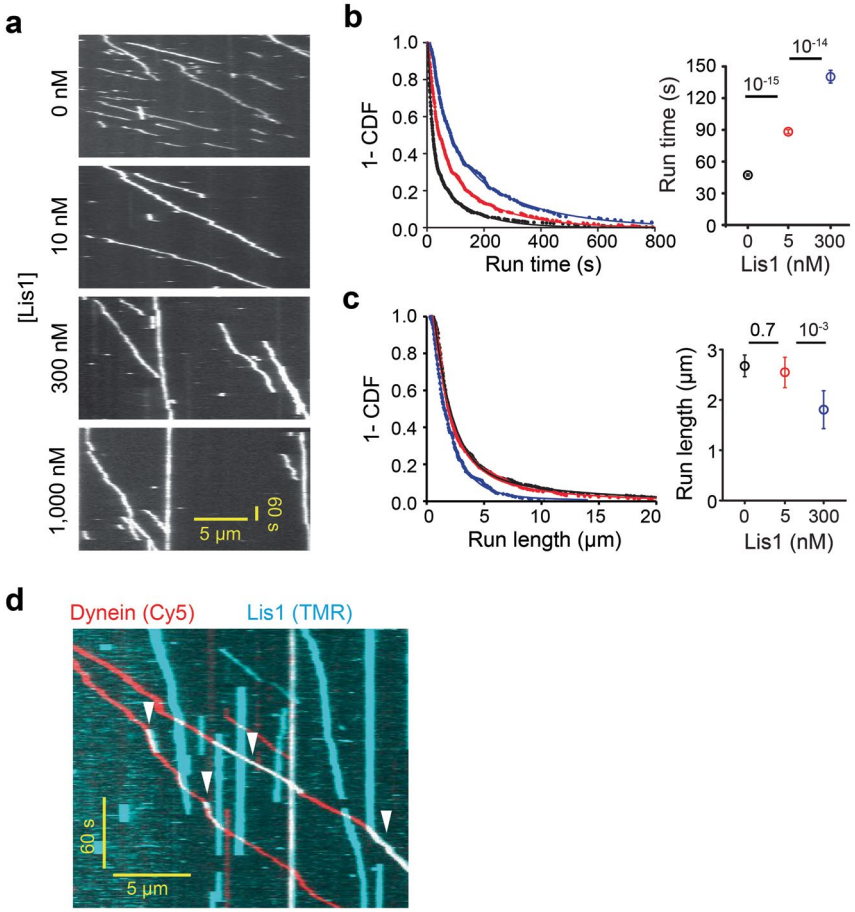

Extended Data Fig. 1 | Single molecule motility of dynein in the presence of Lis1. a) Representative kymographs of TMR-dynein with increasing concentrations of unlabeled Lis1. **b**) (Left) 1-CDF of run time under different Lis1 concentrations. Fitting to a double exponential decay (solid curves) reveals the weighted average of run time in each condition. (Right) The weighted average of run time under increasing Lis1 concentrations (± s.e.; N = 861, 534, and 312 from left to right). **c**) (Left) 1-CDF of run length under different Lis1 concentrations. Solid curves represent a fit to a double exponential decay. (Right) The weighted average of run length in each condition (bar graphs, ± s.e.; N = 861, 534, and 312 from left to right). **d**) An example kymograph shows that the transient binding of Lis1 slows whereas the subsequent release of Lis1 restores the velocity (arrowheads). In **b** and **c**, P values were calculated by the two-tailed Kolmogorov-Smirnov test.

https://doi.org/10.1038/s41589-023-01464-6

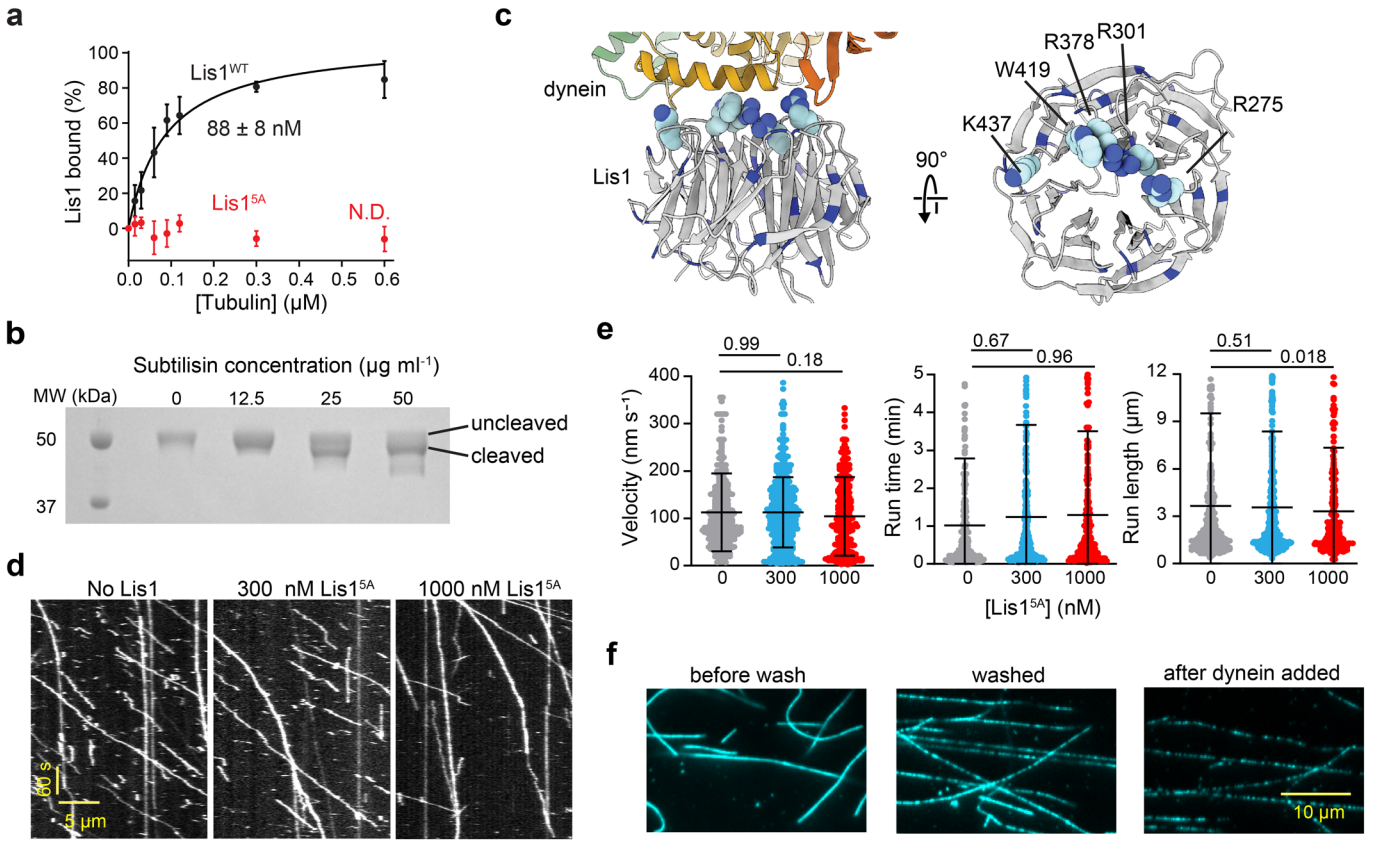

Extended Data Fig. 2 | Lis1 interacts with the microtubule lattice through its dynein binding site in vitro. a) Microtubule co-pelleting assay with Lis1^{WT} and Lis1^{5A} (mean ±s.e.m., three replicates per condition). The solid curve represents a fit to a binding isotherm to determine K_D (±s.e.; N.D.: not determined). The statistical analysis was performed using an extra sum-of-squares F test ($p = 10^{-4}$). **b**) The subtilisin treatment of microtubules reduces the molecular weight of tubulin in a denaturing gel (three independent experiments). **c**) The structure of Lis1 bound to the AAA ring with the five residues mutated in Lis1^{5A} are shown as spheres and all lysine and arginine residues are in blue (Protein Data Bank: 7MGM[15]). **d**) Representative kymographs of dynein in the presence and absence of Lis1^{5A}. Assays were performed in 50 mM KAc. **e**) The velocity, run time, and run length of dynein in the presence and absence of Lis1^{5A} (N = 326, 534, and 336 from left to right). The center line and whiskers represent the mean and s.d., respectively. P values were calculated by a two-tailed t-test with Welch correction for velocity and by the two-tailed Kolmogorov-Smirnov test for run time and run length. **f**) Surface-immobilized microtubules were decorated by 100 nM TMR-Lis1 before and after removing unbound Lis1 in the flow chamber. The assay was performed in the absence of added salt to maximize the Lis1-microtubule interaction. Washing the chamber with buffer and introducing dynein reduces 92% of the Lis1 signal on microtubules (three independent experiments).

https://doi.org/10.1038/s41589-023-01464-6

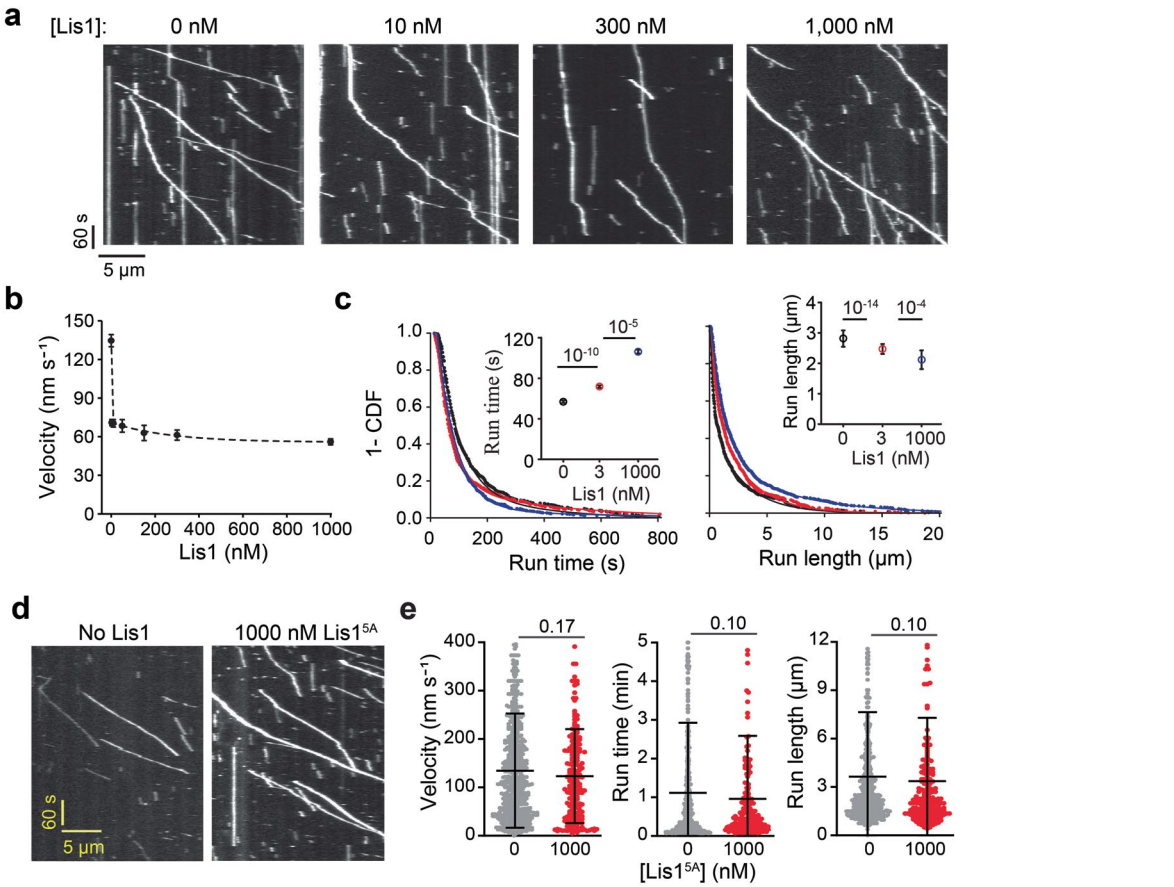

Extended Data Fig. 3 | Motility of dynein$_{Gal}$ in the presence of unlabeled Lis1. **a**) Representative kymographs of dynein$_{Gal}$ with increasing concentrations of unlabeled Lis1. Assays were performed in 1 mM ATP and 150 mM KAc. **b**) The velocity of dynein$_{Gal}$ under different Lis1 concentrations (mean ± s.e.m.; N = 611, 694, 230, 260, 251, and 852 from left to right; two biological replicates). **c**) 1-CDF of run time and run length of dynein$_{Gal}$ under different Lis1 concentrations. Fitting to a double exponential decay (solid curves) reveals the weighted average of run time and run length of the motor in each condition (bar graphs, ± s.e.; N = 611, 694, and 852 from left to right). **d**) Representative kymographs of dynein$_{Gal}$ in the presence or absence of 1,000 nM unlabeled Lis1^{5A}. **e**) The velocity, run time, and run length of dynein$_{Gal}$ in the presence or absence of 1,000 nM Lis1^{5A} (N = 610 and 209 from left to right). The center line and whiskers represent the mean and s.d., respectively. In **c** and **e**, P values were calculated by a two-tailed t-test with Welch correction for velocity and by the two-tailed Kolmogorov-Smirnov test for run time and run length.

https://doi.org/10.1038/s41589-023-01464-6

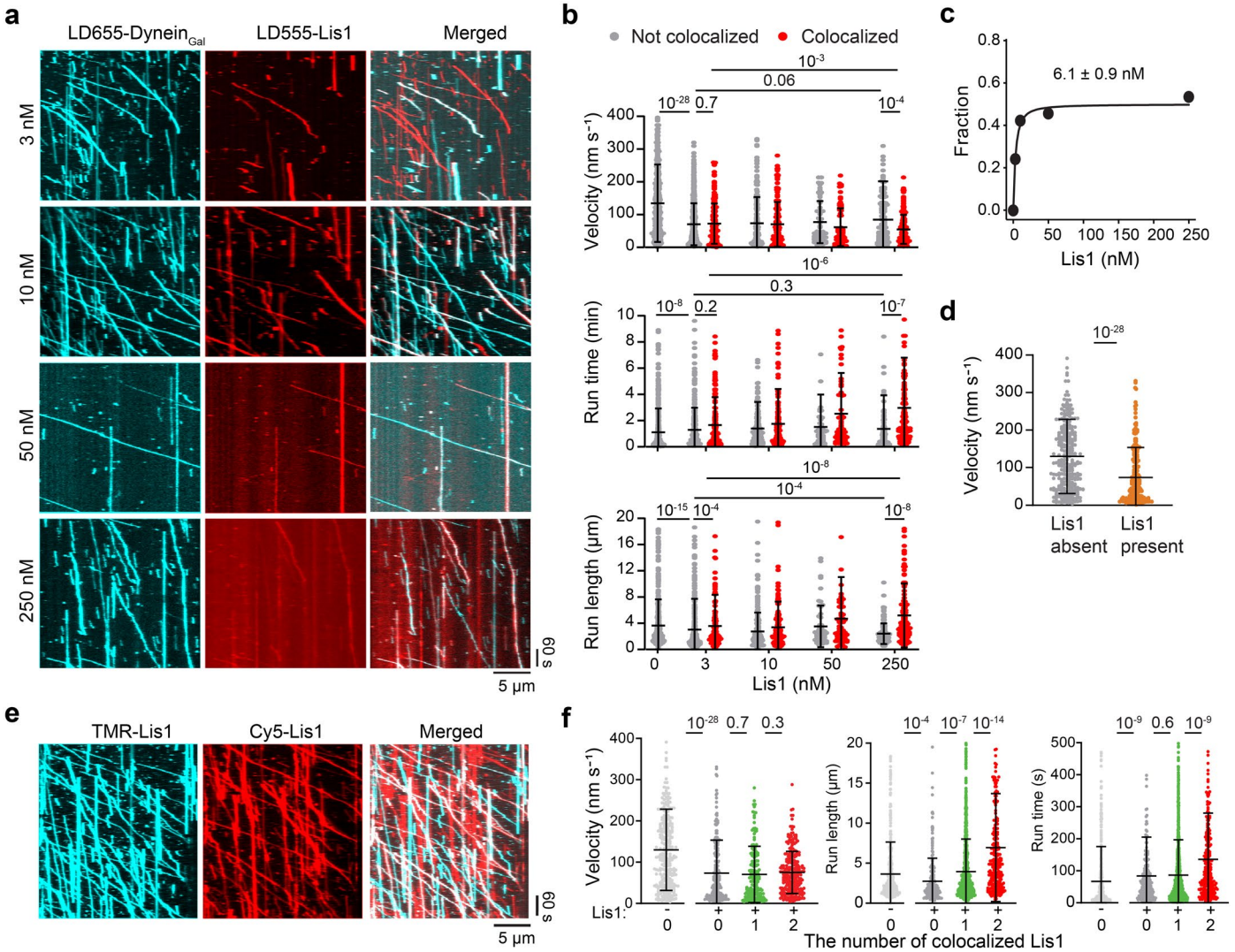

Extended Data Fig. 4 | Motility of dynein$_{Gal}$ in the presence of fluorescently-labeled Lis1. a) Representative kymographs of two-color imaging of LD655-labeled dynein$_{Gal}$ and LD555-labeled Lis1 under different Lis1 concentrations. **b**) The velocity, run time, and run length distributions of dynein$_{Gal}$ under different concentrations of Lis1 (N = 611, 526, 168, 233, 175, 55, 69, 126, and 145 from left to right). **c**) The fraction of LD655-dynein$_{Gal}$ that colocalizes with LD555-Lis1 under different Lis1 concentrations. A fit to a binding isotherm function (solid curve, see Methods) reveals K_D (±s.e.). **d**) The velocity distribution of dynein$_{Gal}$ in the absence of Lis1 compared to the motors that do not colocalize with Lis1 when fluorescently labeled Lis1 is present in the chamber (N = 611 and 233 from left to right). **e**) Representative kymographs show colocalization of 5 nM TMR-labeled and 5 nM Cy5-labeled Lis1 to unlabeled dynein$_{Gal}$. **f**) Velocity, run length, and run time distributions of dynein$_{Gal}$ in the absence (light gray) and presence of Lis1 (N = 287, 233, 175, and 274 from left to right). Dynein$_{Gal}$ motors that colocalize with 0, 1, or 2 colors of Lis1 were analyzed separately. In **b**, **d**, and **f**, the center line and whiskers represent the mean and s.d., respectively. P values were calculated by two-tailed t-tests with Welch correction for velocity and by the two-tailed Kolmogorov-Smirnov test for run time and run-length measurements.

https://doi.org/10.1038/s41589-023-01464-6

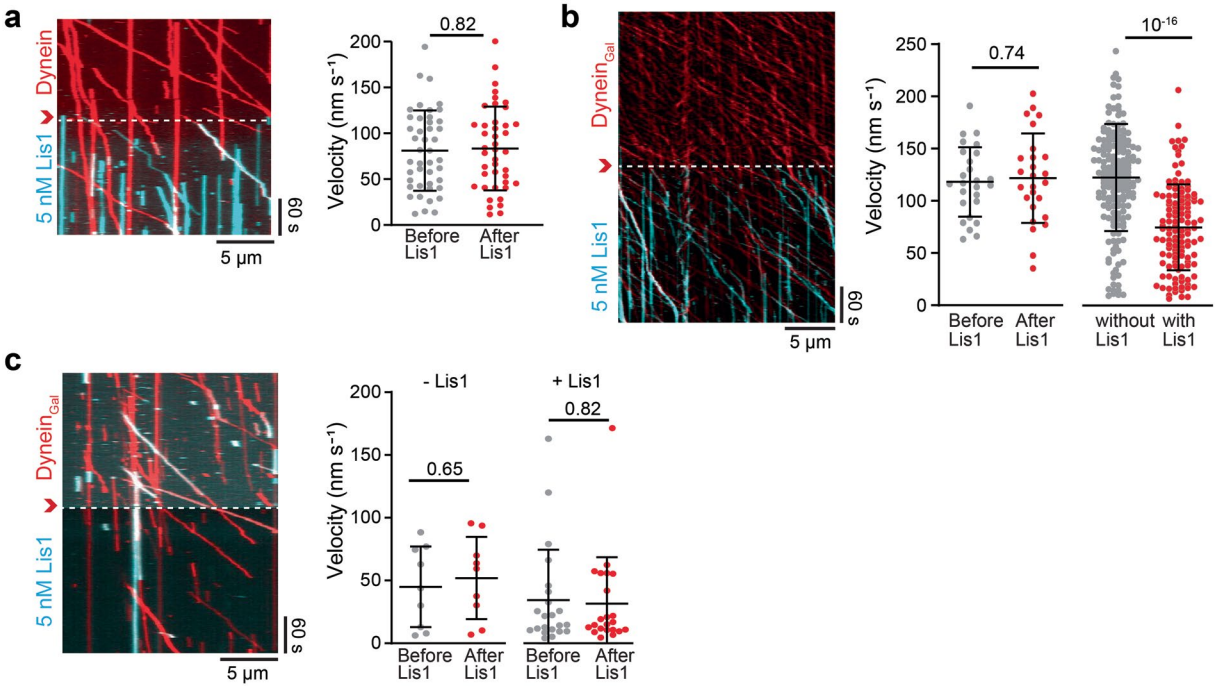

Extended Data Fig. 5 | The addition and removal of Lis1 whilst recording dynein motility. a) A kymograph (left) and velocity (right) of dynein before and after Lis1 was flown into the chamber (red arrowhead and a dashed line, N = 44 and 42 from left to right). **b**) A kymograph of dynein$_{Gal}$ when Lis1 was flown into the chamber (red arrowhead and a dashed line). (Middle) The velocity of the complexes that were already walking on the microtubules during Lis1 addition moved at the same velocity after flowing Lis1 (N = 26 and 26 from left to right). Only the motors that do not colocalize with Lis1 were included in the analysis. (Right) The velocity of the complexes that land onto microtubules within 4 min after Lis1 addition was analyzed (N = 122 and 84 from left to right). The motors that colocalize with Lis1 walked slower than motors that do not colocalize with Lis1. **c**) A kymograph (left) and velocity (right) of dynein$_{Gal}$ before and after washing excess Lis1 from the flow chamber (red arrowhead and a dashed line). The velocity of the motors that colocalize (+Lis1) or do not colocalize (−Lis1) with Lis1 remained unaltered by removing excess Lis1 from the chamber (N = 9, 9, 22, 22 from left to right). In **a**, **b**, and **c**, assays were performed in 1 mM ATP and 50 mM KAc. The center line and whiskers represent the mean and s.d., respectively. P values were calculated by a two-tailed t-test with Welch correction.

https://doi.org/10.1038/s41589-023-01464-6

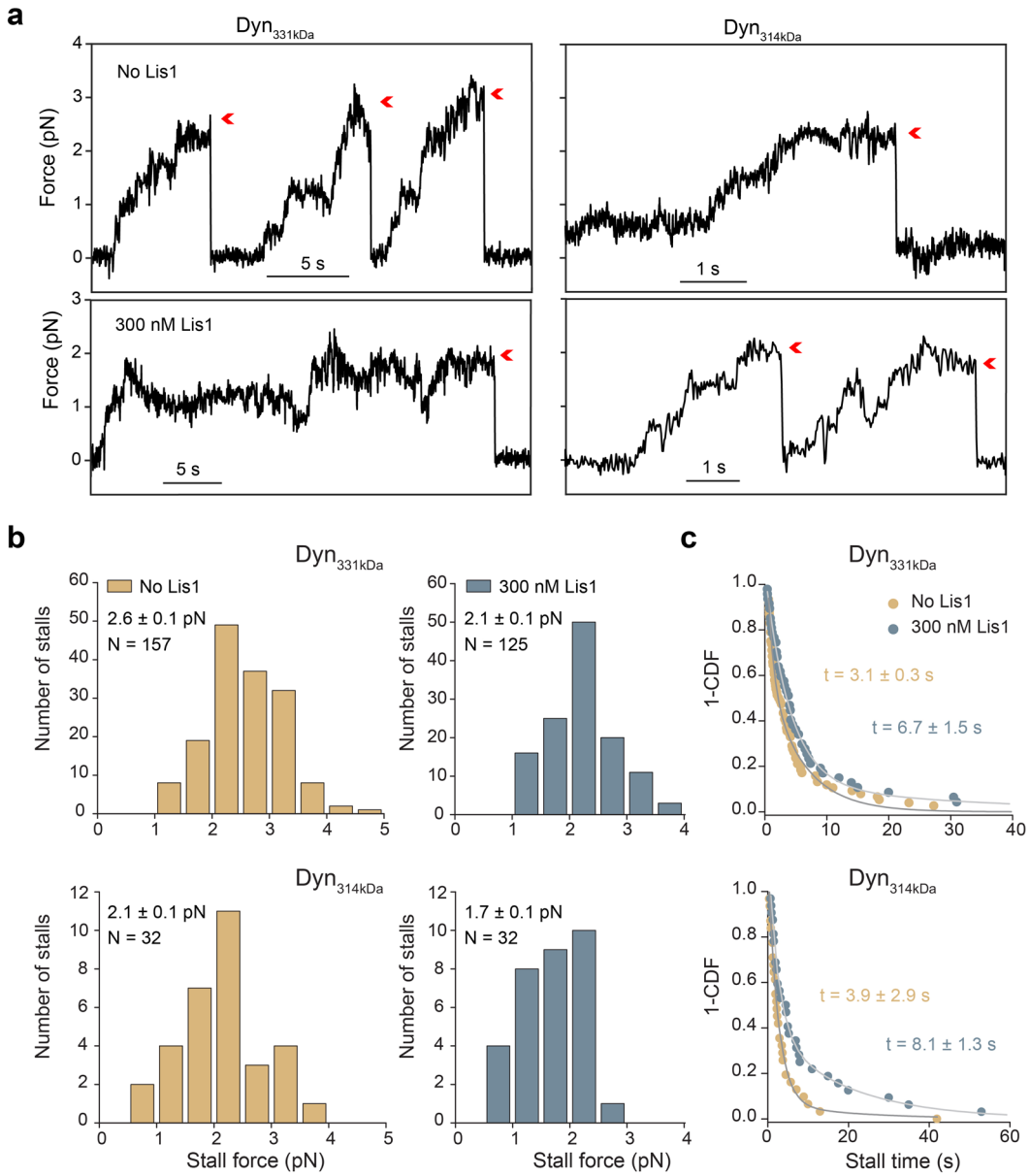

Extended Data Fig. 6 | Lis1 reduces the stall force of the tail-truncated dynein. a) Representative trajectories of beads driven by tail-truncated dynein constructs dimerized with a Glutathione S-transferase (GST) tag (GFP-GST-Dyn_{331kDa} and GFP-GST-Dyn_{314kDa}) in the presence and absence of 300 nM Lis1. Assays were performed in 2 mM ATP. Red arrowheads represent the detachment of the motor from the microtubule followed by the snapping back of the bead to the trap center. **b**) Stall force histograms of Dyn_{331kDa} and Dyn_{314kDa} in the presence and absence of 300 nM Lis1 (mean ± s.e.m.; $p = 2 \times 10^{-7}$ for Dyn_{331kDa} and 0.006 for Dyn_{314kDa}, two-tailed t-test). **c**) Stall times of Dyn_{331kDa} and Dyn_{314kDa} in the presence and absence of 300 nM Lis1. Fitting to a double exponential decay (solid curves) reveals the weighted average of stall time (±s.e.).

https://doi.org/10.1038/s41589-023-01464-6

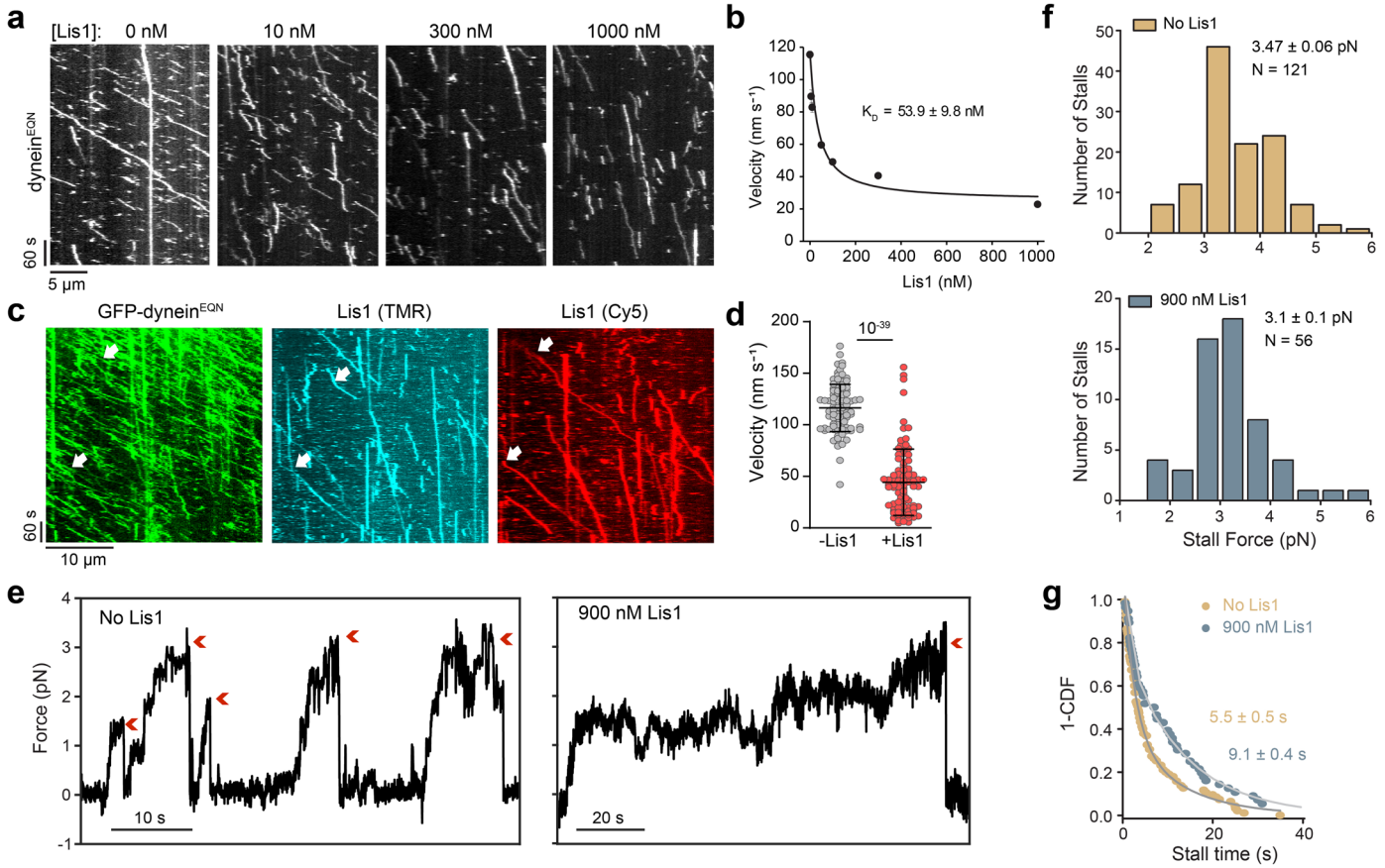

Extended Data Fig. 7 | Lis1 slows the motility but does not substantially affect the stall force of dynein^{EQN}. **a**) Representative kymographs of dynein^{EQN} motility under different concentrations of unlabeled Lis1. **b**) The velocity of dynein^{EQN} motility under different concentrations of unlabeled Lis1 (mean ± s.e.m.; N = 659, 283, 482, 484, 487, 610, and 132 from left to right). The fit of the dynein^{EQN} velocity data (solid curve) reveals K_D (±s.e., see Methods). **c**) A representative kymograph of a three-color imaging assay shows two Lis1s bind to the same dynein^{EQN} motor (white arrows). **d**) The velocities of dynein^{EQN} motors not colocalizing (-Lis1) or colocalizing (+Lis1) with Lis1 (N = 98 and 92 from left to right). The center line and whiskers represent the mean and s.d., respectively. The P-value was calculated by a two-tailed t-test with Welch correction. **e**) Representative trajectories of beads driven by dynein^{EQN} in the presence or absence of 900 nM Lis1 in a fixed trapping assay. Assays were performed in 2 mM ATP. Red arrowheads represent the detachment of the motor from the microtubule followed by the snapping back of the bead to the trap center. **f**) Stall force histograms of dynein^{EQN} in the presence and absence of 900 nM Lis1 (mean ± s.e.m.; $p = 10^{-3}$, two-tailed t-test). **g**) Stall times of dynein^{EQN} in the presence and absence of 900 nM Lis1. Fitting to a double exponential decay (solid curves) reveals the weighted average of stall time (±s.e.).

https://doi.org/10.1038/s41589-023-01464-6

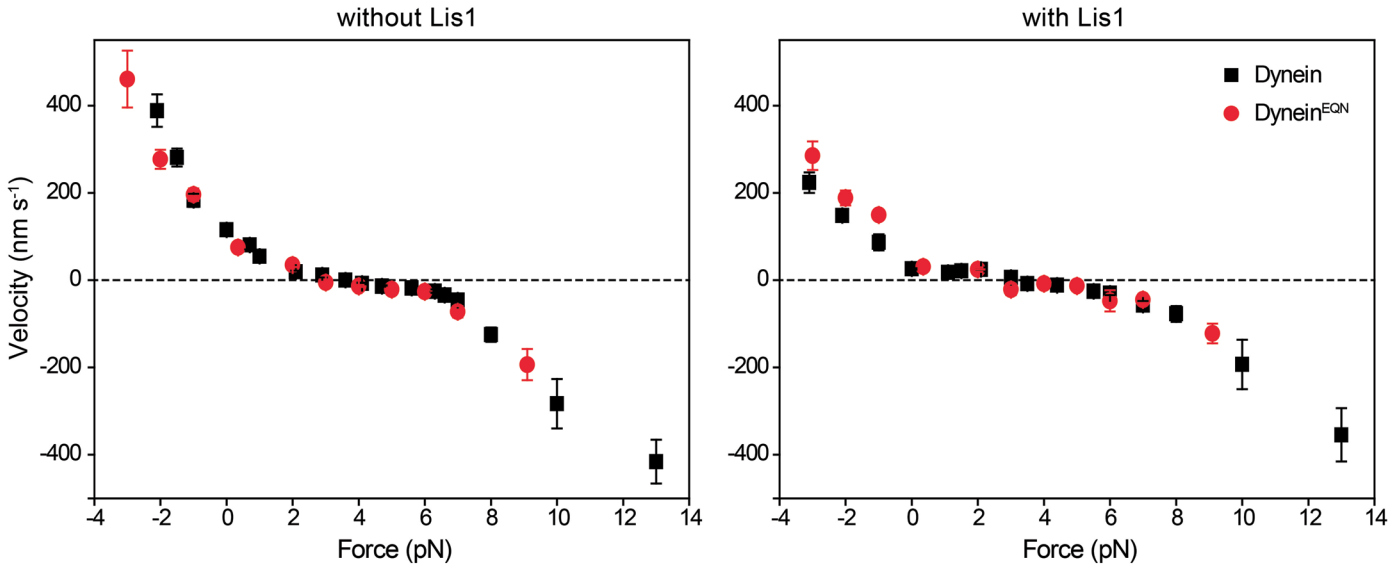

Extended Data Fig. 8 | The comparison of the F-V behavior of dynein and dynein^{EQN} in the presence and absence of Lis1. (Left) F-V measurements of dynein and dynein^{EQN} in the absence of Lis1 (mean ±s.e.m., from left to right, N = 41, 38, 37, 861, 27, 52, 106, 28, 51, 60, 89, 115, 124, 62, 23, 38, 40 for dynein and N = 31, 66, 62, 48, 47, 26, 42, 39, 23, 45, 33 for dynein^{EQN}). (Right) F-V measurements of dynein in 300 nM Lis1 compared to F-V of dynein^{EQN} in 900 nM Lis1 (mean ±s.e.m., from left to right, N = 34, 52, 25, 312, 33, 42, 49, 37 62, 47 33 42, 36, 29, 18 for dynein; and N = 54, 36, 61, 31, 37, 17, 54, 14, 19, 38, 26 for dynein^{EQN}). Dynein velocity under assisting forces is lower than that of dynein^{EQN} in the presence of Lis1. Assays were performed in 2 mM ATP.

nature portfolio

Corresponding author(s): Ahmet Yildiz

Last updated by author(s): Sep 14, 2023

Reporting Summary

Nature Portfolio wishes to improve the reproducibility of the work that we publish. This form provides structure for consistency and transparency in reporting. For further information on Nature Portfolio policies, see our Editorial Policies and the Editorial Policy Checklist.

Statistics

For all statistical analyses, confirm that the following items are present in the figure legend, table legend, main text, or Methods section.

n/a	Confirmed
☐	☒ The exact sample size (*n*) for each experimental group/condition, given as a discrete number and unit of measurement
☐	☒ A statement on whether measurements were taken from distinct samples or whether the same sample was measured repeatedly
☐	☒ The statistical test(s) used AND whether they are one- or two-sided *Only common tests should be described solely by name; describe more complex techniques in the Methods section.*
☐	☒ A description of all covariates tested
☐	☒ A description of any assumptions or corrections, such as tests of normality and adjustment for multiple comparisons
☐	☒ A full description of the statistical parameters including central tendency (e.g. means) or other basic estimates (e.g. regression coefficient) AND variation (e.g. standard deviation) or associated estimates of uncertainty (e.g. confidence intervals)
☐	☒ For null hypothesis testing, the test statistic (e.g. *F*, *t*, *r*) with confidence intervals, effect sizes, degrees of freedom and *P* value noted *Give P values as exact values whenever suitable.*
☒	☐ For Bayesian analysis, information on the choice of priors and Markov chain Monte Carlo settings
☒	☐ For hierarchical and complex designs, identification of the appropriate level for tests and full reporting of outcomes
☒	☐ Estimates of effect sizes (e.g. Cohen's *d*, Pearson's *r*), indicating how they were calculated

Our web collection on statistics for biologists contains articles on many of the points above.

Software and code

Policy information about availability of computer code

Data collection	Labview 2017 was used for hardware control of the optical trap instrument. Micro-Manager 2.0 was used for image acquisition.
Data analysis	Fiji 1.0 was used to analyze TIRF images. Matlab 2019a was used to process and analyze optical trap data. Figures were plotted using Fiji 1.0, Matlab 2019a, and Origin Pro 9.0. Custom codes developed in this study were uploaded to the Yildiz Lab github repository.

For manuscripts utilizing custom algorithms or software that are central to the research but not yet described in published literature, software must be made available to editors and reviewers. We strongly encourage code deposition in a community repository (e.g. GitHub). See the Nature Portfolio guidelines for submitting code & software for further information.

Data

Policy information about availability of data

All manuscripts must include a data availability statement. This statement should provide the following information, where applicable:

- Accession codes, unique identifiers, or web links for publicly available datasets
- A description of any restrictions on data availability
- For clinical datasets or third party data, please ensure that the statement adheres to our policy

A reporting summary for this article is available as Supplementary Information file. The main data supporting the findings of this study are available within the article and its Supplementary Figures. Additional details on datasets and protocols that support the findings of this study will be made available by the corresponding authors upon reasonable request.

Human research participants

Policy information about studies involving human research participants and Sex and Gender in Research.

Reporting on sex and gender	N/A
Population characteristics	N/A
Recruitment	N/A
Ethics oversight	N/A

Note that full information on the approval of the study protocol must also be provided in the manuscript.

Field-specific reporting

Please select the one below that is the best fit for your research. If you are not sure, read the appropriate sections before making your selection.

☒ Life sciences ☐ Behavioural & social sciences ☐ Ecological, evolutionary & environmental sciences

For a reference copy of the document with all sections, see nature.com/documents/nr-reporting-summary-flat.pdf

Life sciences study design

All studies must disclose on these points even when the disclosure is negative.

Sample size	In each experiment (single imaging slide) and 5 random fields of view were chosen and the number of molecules or microtubules in these fields of view determine the sample size per measurement. The sample sizes we obtained from these measurements were sufficient to reduce the standard of the mean to at least 1/4th of the mean value.
Data exclusions	For single molecule motility assays, diffusive molecules and molecules with short run lengths (< 2 pixels or < 200 nm) or paused for more than 1 sec were excluded from the velocity analysis. In optical trap assays, attachments that are shorter than 100 ms were excluded from the analysis.
Replication	Experiments were performed over the course of several months. All experiments were successfully replicated and each representative image / kymograph 'n' value represents the number of biologically distinct samples (molecules or microtubules). The number of experiments performed are given in the figure legends.
Randomization	All biological samples including proteins, microtubles, and additional assay components were aliquoted into small volumes and randomly allocated into different experimental groups. For experiments, random field of views were selected during imaging and either all events in the field of view or all events on a random microtubule were analyzed.
Blinding	Experiments were inherently blinded since it is impossible to select subpopulations of molecules, microtubules, or assay components from stock solutions when pipetting.

Reporting for specific materials, systems and methods

We require information from authors about some types of materials, experimental systems and methods used in many studies. Here, indicate whether each material, system or method listed is relevant to your study. If you are not sure if a list item applies to your research, read the appropriate section before selecting a response.

Materials & experimental systems

n/a	Involved in the study
☐	☒ Antibodies
☒	☐ Eukaryotic cell lines
☒	☐ Palaeontology and archaeology
☒	☐ Animals and other organisms
☒	☐ Clinical data
☒	☐ Dual use research of concern

Methods

n/a	Involved in the study
☒	☐ ChIP-seq
☒	☐ Flow cytometry
☒	☐ MRI-based neuroimaging

Antibodies

Antibodies used

Custom made rabbit polyclonal GFP antibody (Covance, CA 5314/15) were purified by GFP affinity chromatography and 1 mg/ml antibody was used for coating carboxyl latex beads (Life Technologies) for optical trapping assays.

Validation

Custom made rabbit polyclonal GFP antibody (Covance, CA 5314/15) were verified by the ELISA screening assay performed by the supplier. In an ELISA, the specific binding between an antigen and antibody is measured using a secondary enzyme labeled antibody and substrate system and is reported as 50% titer. The antbodies were affinity purified by a GFP column, and their binding to recombinantly expressed eGFP was verified using Western Blotting in our laboratory. The antibody was used for linking pure GFP-tagged protein to polystyrene beads in the absence of other proteins.